Dimensionality Aspects of Adaptive Radar Pulse Compression

by

Thomas Higgins

Submitted to the Department of Electrical Engineering and Computer Science
and the Faculty of the Graduate School of the University of Kansas
In partial fulfillment of the requirements for the degree of Master's of Science

_____

Dr. Shannon Blunt (Chair)

_____

Dr. James Stiles

_____

Dr. Christopher Allen

Date Defended:_____

The Thesis Committee for Thomas Higgins certifies
That this is the approved version of the following thesis:

Dimensionality Aspects of Adaptive Radar Pulse Compression

_____

Dr. Shannon Blunt (Chair)

_____

Dr. James Stiles

_____

Dr. Christopher Allen

Date Approved:_____

Acknowledgements

First and foremost, I would like to thank Dr. Blunt for allowing me to work under him and inspiring me to be curious and creative. Dr. Blunt has expanded my knowledge, on an almost daily basis, by taking the time to explain and answer any questions I bring to him. He has provided me the opportunity to work with him on a pending journal article and two accepted conference papers as well as funding my travel to two of the IEEE National Radar Conferences. I would like to thank Dr. Stiles for being an excellent teacher who cares about his students and also for introducing me to Dr. Blunt. I am positive that no student has ever left Dr. Stiles' office with an unsatisfactory answer to a question. Also, I want to thank Dr. Allen whose great personality and vast knowledge of radar makes him an invaluable teacher, committee member, and target for my questions. I wish to thank my friends and fellow students in the Radar Systems Lab (Bill, Charley, Geoff, Jamie, Kevin, and Padmaja) for their meaningful insight and discussion. Last but certainly not least, I would like to thank my parents for their vast amount of encouragement and financial support as well as my sisters Shannon and Katie for their emotional support.

Abstract

Adaptive filtering for radar pulse compression has been shown to greatly improve sidelobe suppression through the estimation of an appropriate pulse compression filter for each individual range cell of interest. However, the relatively high computational cost of full-dimension adaptive range processing may limit practical implementation in many current real-time systems. In this thesis, dimensionality reduction techniques are employed to approximate the framework for pulse compression filter estimation. Two new algorithms denoted as specific embodiments of the Fast Adaptive Pulse Compression (FAPC) method are shown to maintain performance close to that of full-dimension adaptive processing while significantly reducing computation cost.

Conversely, over-sampling the received radar return and transmit waveform used for processing enables increased-dimensionality adaptive filtering to achieve range super-resolution on a single pulse basis. This thesis analyzes the effects of continuous and realistic discrete waveforms in the context of range super-resolution.

Table of Contents

CHAPTER 1 INTRODUCTION

1.1 Radar Background

Pulsed radars are used for a wide variety of applications and typically emit several short pulses of electromagnetic energy. The energy reflected back in the direction of the system is gathered and processed to determine information such as range and radar cross section (RCS) of the scatterers or targets illuminated by the radar. Range and RCS can be easily determined by the round trip travel time and energy of the received reflections, respectively. The received energy determines the signal-to-noise ratio (SNR) characteristics of the system [1] which is closely related to the system's ability to detect low RCS targets. Range resolution is defined as the minimum distance, with respect to a radial line outward from the antenna, required between targets such that they are distinguishable in range. The range resolution is inversely proportional to the bandwidth of the transmitted signal *i.e.* increasing transmitted bandwidth improves resolution [1]. The illuminated area can be separated into range cells each of which has a length equal to the range resolution, *i.e.* point targets must have at least one range cell between them to be separable. The collection of range cells that are of interest will be referred to as the range profile in this thesis. In practice, pulsed radars often utilize a technique called pulse compression to

achieve the desired range resolution and SNR performance. The next section will provide a brief explanation of pulse compression and discuss some aspects of pulse compression waveforms and filters

1.2 Pulse Compression

The energy and bandwidth of the transmitted pulse determines the SNR and range resolution characteristics of the radar system, respectively. A short pulse with high peak power can provide both adequate energy and bandwidth, but is impractical and costly to implement because of the need for a high power source and components which can tolerate a wide dynamic range of power. Pulse compression is a widely known technique which is used to achieve the energy and bandwidth characteristics of a short high power pulse with a longer low power modulated waveform by appropriately filtering the received signal [1]. The product of the power and pulse duration equates to the transmitted energy, *i.e.* a low power waveform with relatively long duration can provide the same energy, and thus SNR, found in a short higher power transmit signal. Also, the high bandwidth of a temporally short pulse can be achieved by phase or amplitude modulation of a longer pulse. Amplitude modulation is seldom used in practice because it is less efficient, in terms of transmitted energy, than a constant modulus waveform.

When a longer waveform is utilized a pulse compression filter is necessary to obtain the enhanced SNR and range resolution discussed above. Fig 1.1 depicts a received radar signal before pulse compression and Fig 1.2 displays the resulting profile estimate after pulse compression. Note that it is not evident in Fig. 1.1 that two targets are present however, after a pulse compression filter is applied the range resolution and SNR is improved and the two targets can easily be resolved as seen in Fig. 1.2. Although pulse compression alleviates the need for high power transmitters and components, waveform selection and processing techniques become pertinent. The following two sections will provide a brief background of pulse compression waveforms and filters.

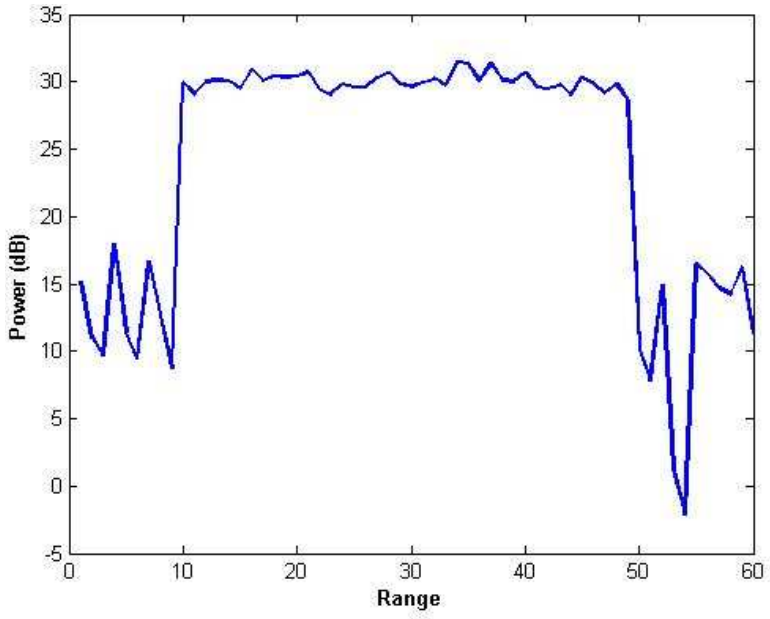

Figure 1.1 Received Radar Signal Before Pulse Compression

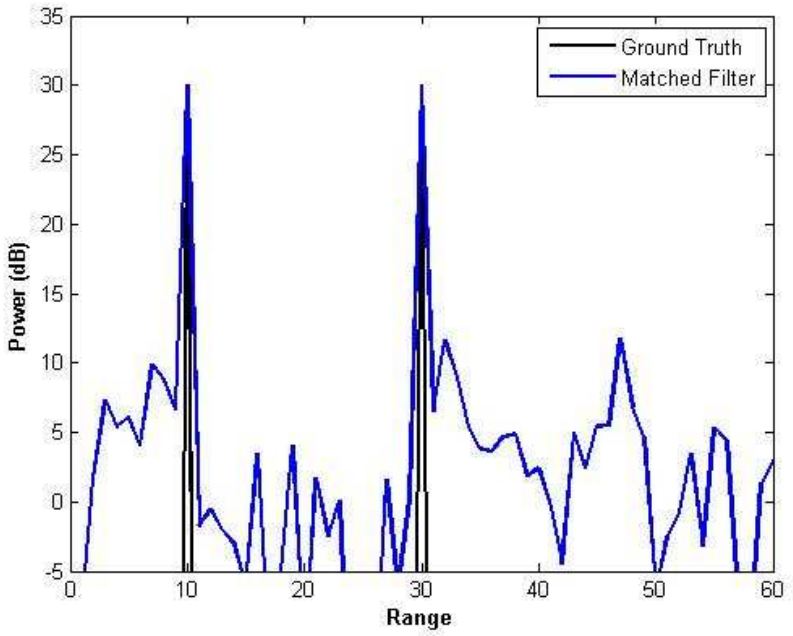

Figure 1.2 Received Radar Signal After Pulse Compression

1.2.1 The Matched Filter

Pulse compression is often achieved by filtering the received signal with a time-reversed conjugate of the transmitted waveform or equivalently correlating the received signal and transmitted waveform. This widely used technique is referred to as matched filtering because the filter is matched to the transmit waveform. It is well known that the matched filter maximizes the SNR for a single point target in white noise [2]. In the previous example a normalized version of the matched filter was applied to the received signal in Fig. 1.1 to produce the range profile seen in Fig. 1.2.

The matched filter transforms the received signal from delayed, attenuated versions of the transmitted waveform to delayed, attenuated versions of the

autocorrelation of the waveform. Fig. 1.3 shows the normalized autocorrelation of a length $N = 20$ Lewis-Kretschmer P3 code [3], which is a discrete version of a phase modulated waveform. Note that the autocorrelation contains sidelobes which are approximately 20 dB below the peak. Hence when a large target is present the autocorrelation sidelobes of the transmitted waveform may mask smaller targets in the surrounding range cells. However, the digital matched filter is computationally efficient enough to implement in real-time systems requiring only $O(N)$ (where N is the discretized length of the transmitted waveform) multiplies to compute the complex amplitude estimate at each range cell of interest.

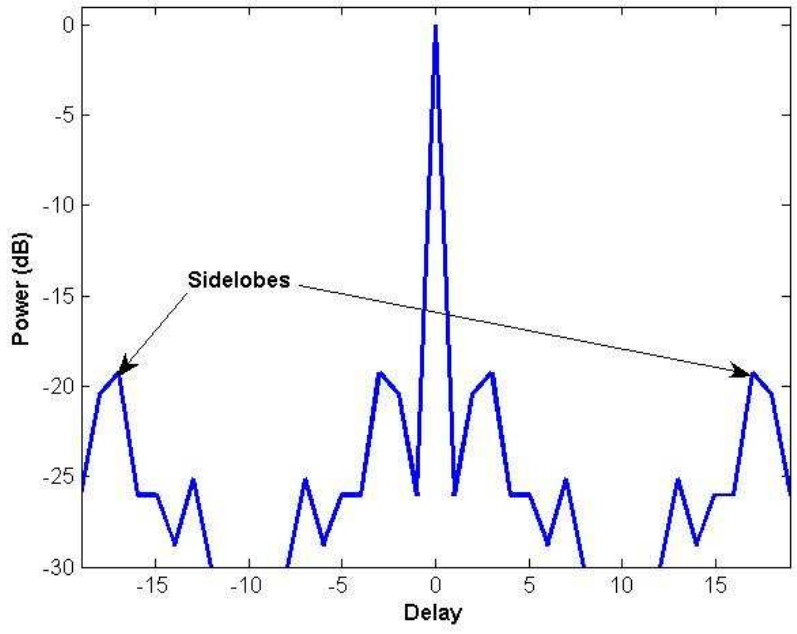

Figure 1.3 Auto-Correlation of P3 Code

1.2.2 Waveform Design

There has been extensive research done in the field of waveform design to determine those which exhibit low autocorrelation sidelobes. The most commonly used pulse compression waveform is a linear frequency modulation (LFM) waveform more often referred to as a chirp. Chirp waveforms usually employ frequency modulation (as opposed to amplitude modulation) thus maintaining a constant modulus throughout the duration of the pulse. Discrete phase waveforms are gaining popularity as digital systems become more prevalent. Binary phase-coded waveforms [2], which are limited to the discrete phase values of 0 and π, must be optimized for a given length discrete waveform but can provide excellent sidelobe characteristics. Polyphase codes are similar to binary phase-coded waveforms without the phase restrictions. The Lewis-Kretschmer P3 code utilized in Fig. 1.3 is a polyphase code which essentially approximates a sampled (at the Nyquist rate) version of a continuous time LFM waveform. It should be noted that randomly generated binary phase codes usually exhibit poor sidelobe characteristics whereas, random polyphase codes generally yield low sidelobe levels. Other types of waveforms that have been explored include non-linear frequency modulation waveforms [4]-[5], Costas codes [6], complementary codes [7], and Frank codes [8]. While the aforementioned waveforms reduce sidelobe levels each has its own advantages and disadvantages. Waveforms with other advantageous properties such as low probability of intercept (LPI) or Doppler tolerance may not necessarily have

desirable sidelobe characteristics. The transmit waveform is a vital component to pulse compression processing even when the filter is not matched to it.

1.2.3 Other Filtering Techniques

Signal processing techniques have been utilized to develop pulse compression filters that exhibit sidelobe mitigation. The Least-Squares approach [9] de-correlates the waveform with delayed versions of itself and thus side lobe interference from surrounding range cells. Inverse filters, which have a frequency response that approximates the inverse response of the transmitted waveform, have also been explored [10]. Optimum mismatched filters [11] have been derived using a constrained Least-Squares approach. As mentioned earlier the matched filter maximizes SNR, and thus detection, for a solitary point target in noise hence one must consider this optimality when exploring new approaches to pulse compression filtering.

Recently, a new adaptive approach to pulse compression was proposed which, unlike the aforementioned deterministic receive techniques, determines the particular receive filter to employ for each individual range cell thus greatly suppressing sidelobe levels with little loss in SNR. Denoted as Adaptive Pulse Compression (APC) [12] this approach is capable of adaptively suppressing range sidelobes from large scatterers into the noise thus unmasking nearby small scatterers. The elimination of range sidelobes is achieved by adaptively estimating the pulse compression filter to use for each range cell by employing

relative power estimates of the surrounding range cells that are obtained initially from the output of the matched filter. For a given range cell the respective filter places nulls at range offsets relative to nearby large scatterers thus suppressing the range sidelobes that are induced by the large targets. Unlike the matched filter some of the aforementioned digital processing techniques are capable of achieving range super-resolution.

1.3 Range Super-Resolution

Super-resolution in this thesis refers to resolution enhancement achieved through processing techniques that do not alter the resolution-determining parameters of the system, *e.g.* enhancing radar range resolution without increasing the bandwidth of the transmitted waveform. Super-resolution has been achieved in the spatial and spectral domains using eigen-decomposition subspace approaches such as MUSIC and ESPIRIT [13]. In the spatial/spectral domains the signals which are being discerned are assumed to be at different angles/frequencies whereas super-resolution in the range domain involves discerning between two identical signals albeit at different delays and magnitudes. Thus the aforementioned spatial/spectral super-resolution techniques have not been applied to achieve range super-resolution. However, the methods proposed by Gabriel in [14]-[15] show that range super-resolution can be achieved by employing a Weiner based solution wherein a sample covariance matrix from several pulses is utilized to perform interference cancellation. The Least-Squares

algorithm has also been utilized to achieve range super-resolution [16] using only a single pulse. Later it will be shown that an over-sampled version APC is capable of super-resolution on a single pulse basis.

1.4 Motivation

The APC algorithm has been shown [12] to be superior to both standard matched filtering and Least-Squares based mismatched filtering as well as potentially enabling the use of waveforms which provide sub-optimum sidelobe level performance yet possess other desirable characteristics such as LPI. Of course, the sidelobe suppression capability of APC is commensurate with the sidelobe properties of a given waveform and thus there remains a benefit to employing waveforms with inherently low sidelobes and Doppler tolerance. The APC algorithm also enables range super-resolution when the transmit waveform and received signal are over-sampled.

The performance benefit of full-dimension adaptive processing approaches such as the APC algorithm is obtained at the cost of higher computational complexity. For example, given a transmit waveform with a discretized length of N samples, the computational cost of standard matched filtering is $O(N)$, while for APC it is $O(N^2)$ (when the efficient implementation from [12] is employed). As a result, the use of APC is limited in current real-time systems.

The enhanced sensitivity provided by the computationally burdensome APC algorithm is desirable in many real-time applications. In this thesis reduced-dimensionality techniques have been utilized to decompose the full-dimension APC signal model thus enabling adaptivity to be performed on a smaller space. From a conceptual standpoint, similar endeavors have been considered for Space-Time Adaptive Processing (STAP) which must also contend with the cost of adapting on a high dimensionality space [17]. By applying dimensionality reduction via a segmented approximation to the original MMSE cost function a new algorithm entitled Fast Adaptive Pulse Compression (FAPC) will be developed. While numerous possible variations of Fast APC exist, this thesis shall consider the two particular embodiments formed using decimation and contiguous blocking techniques. The resulting algorithm maintains enhanced sensitivity over the matched filter and other pulse compression filters with a significantly lower computational cost than full-dimension APC.

The range super-resolution capability of APC offers several distinct advantages to pulsed radar systems. Enhanced resolution techniques offer a solution to limited bandwidth components and the decreasing availability of spectrum by maintaining a desired resolution without high bandwidth requirements. Super-resolution processing algorithms can also be utilized in a multi-mode scenario where the enhanced resolution mode does not impose extraneous bandwidth requirements on the system. Range super-resolution algorithms can be employed to update existing systems as well.

Over-sampling the transmitted waveform used for processing and received signal enables range super-resolution to be achieved when Least-Squares is applied as seen in [16]. The APC algorithm is also capable of achieving super-resolution when over-sampling is utilized. This thesis will analyze the super-resolution capabilities of APC and Least-Squares when the transmitted signal is modeled as either an over-sampled continuous or realistic discrete waveform. Also, diagonal loading will be utilized to alleviate ill-conditioning effects stemming from the over-sampled version of the waveform used for processing.

1.5 Organization of Thesis

The rest of this thesis is organized in the following manner. The remainder of Chapter 1 will present the matched filter, APC, and Least-Squares signal models and filter formulations. The following chapter contains a description of the over-sampled versions of APC and Least-Squares as well as the derivation and analysis of the new Fast APC (FAPC) algorithm. Chapter 3 discusses implementation concerns for the increased and reduced dimensionality algorithms discussed in Chapter 2. Simulation results are presented in Chapter 4 and conclusions and future work are highlighted in Chapter 5.

1.6 Background

This section will provide a brief overview of the matched filter, Adaptive Pulse Compression (APC), and Least-Squares approaches. The first step in constructing a robust signal processing algorithm is obtaining an accurate mathematical interpretation of physical phenomena referred to as the radar return model in this context. The pulsed radar return model is often approximated as a discrete convolution of the transmitted waveform with the range profile. Thus, the received radar return, from a single pulse, at the ℓ^{th} range cell can be approximated as

$$y(\ell) = \mathbf{x}^T(\ell)\mathbf{s} + v(\ell) \tag{1.1}$$

for $\ell = 0,\cdots, L+N-2$, where $\mathbf{s}=\begin{bmatrix} s_0 & s_1 & \cdots & s_{N-1} \end{bmatrix}^T$ is the length N transmit waveform, $\mathbf{x}(\ell) = \begin{bmatrix} x(\ell) & x(\ell-1) & \cdots & x(\ell-N+1) \end{bmatrix}^T$ is the portion of the range profile that the transmitted waveform **s** convolves with at delay ℓ, $\mathbf{v}(\ell)$ is additive noise, $(\bullet)^T$ is the transpose operation, and L is the number of range cells of interest.

1.6.1 Matched Filter and APC Signal Model

The original APC algorithm utilizes the same signal model as the matched filter which is formed by collecting N consecutive samples of the received radar return signal from (1.1), expressed as

$$\mathbf{y}(\ell) = \mathbf{X}^T(\ell)\mathbf{s} + \mathbf{v}(\ell) \tag{1.2}$$

where $\mathbf{v}(\ell) = \left[v(\ell) \quad v(\ell+1) \quad \cdots \quad v(\ell+N-1)\right]^T$ and

$$\begin{aligned}\mathbf{X}(\ell) &= \left[\mathbf{x}(\ell) \quad \mathbf{x}(\ell+1) \quad \cdots \quad \mathbf{x}(\ell+N-1)\right] \\ &= \begin{bmatrix} x(\ell) & x(\ell+1) & \cdots & x(\ell+N-1) \\ x(\ell-1) & x(\ell) & \cdots & x(\ell+N-2) \\ \vdots & \vdots & \ddots & \vdots \\ x(\ell-N+1) & \cdots & x(\ell-1) & x(\ell) \end{bmatrix}.\end{aligned} \tag{1.3}$$

This full-dimension signal model will be referred to when deriving the over-sampled and reduced-dimensionality models.

1.6.2 Matched Filter Formulation

The normalized matched filter estimate of the complex amplitude at the ℓ^{th} range cell in the discrete domain is computed as the inner product

$$\hat{x}_{\text{MF}}(\ell) = \frac{1}{N}\mathbf{s}^H\mathbf{y}(\ell) \tag{1.4}$$

for $\ell = 0,1,\cdots,L-1$, where $(\bullet)^H$ is the complex conjugate transpose (or Hermitian) operation. Matched filtering, which is currently employed in real-time systems, will be utilized as a computational cost and performance comparison metric when discussing the new algorithm, Fast APC, presented in this thesis. The matched filter is computationally efficient but exhibits poor sensitivity in

profiles which contain large targets *i.e.* targets with a SNR above the sidelobe levels of the transmitted waveform.

1.6.3 APC Filter Formulation

The full-dimension APC algorithm from [12] utilizes a reiterative minimum mean squared error (MMSE) framework. The APC cost function in standard MMSE form is given as

$$J(\ell) = E\left[\left|x(\ell) - \mathbf{w}^H(\ell)\mathbf{y}(\ell)\right|^2\right] \tag{1.5}$$

where $\mathbf{w}(\ell)$ is the unique pulse compression filter, which is used to estimate the complex amplitude at the ℓ^{th} range cell $x(\ell)$, $\mathbf{y}(\ell)$ is the received signal, and $E[\bullet]$ is the expectation operator. The cost function is minimized in a typical fashion by differentiating with respect to $\mathbf{w}^*(\ell)$ and setting the result equal to zero. The resulting pulse compression filter at the ℓ^{th} range cell takes the form

$$\mathbf{w}(\ell) = \left(E\left[\mathbf{y}(\ell)\mathbf{y}^H(\ell)\right]\right)^{-1} E\left[\mathbf{y}(\ell)x^*(\ell)\right]. \tag{1.6}$$

Inserting the full-dimension signal model from (1.2) into (1.6) above and assuming the range cells are uncorrelated with the noise and with each other the filter is denoted

$$\mathbf{w}(\ell) = \rho(\ell)\left(\mathbf{C}(\ell) + \mathbf{R}\right)^{-1}\mathbf{s} \tag{1.7}$$

for $\ell = 0,1,\cdots,L-1$, where $\rho(\ell) = E\left[\,|x(\ell)|^2\,\right]$ is the expected power of $x(\ell)$, $\mathbf{R} = E\left[\mathbf{v}(\ell)\mathbf{v}^H(\ell)\right]$ is the full-dimension noise covariance matrix, and the full-dimension signal correlation matrix $\mathbf{C}(\ell)$ is expressed

$$\mathbf{C}(\ell) = \sum_{n=-N+1}^{N-1} \rho(\ell+n)\,\mathbf{s}_n\mathbf{s}_n^H \tag{1.8}$$

where $\mathbf{s}_n$ represents a delay-shifted version of the waveform with the remainder zero-filled, *e.g.* $\mathbf{s}_1 = [0 \quad s_0 \quad \cdots \quad s_{N-2}]^T$ and $\mathbf{s}_{-1} = [s_1 \quad \cdots \quad s_{N-1} \quad 0]^T$. The derivation of the APC filter will be referred to when the new work is presented. The APC algorithm exhibits almost complete sidelobe suppression but is computationally expensive in terms of current processing power. This algorithm will be used as a computational cost and performance comparison metric for Fast APC.

1.6.5 Least-Squares Signal Model and Filter

The Least-Squares system response model approximates the convolution of the range profile with the transmitted waveform as a matrix multiply resulting in the length-$(L+N-1)$ vector $\mathbf{y}_{\mathrm{LS}}$ denoted as

$$\mathbf{y}_{\mathrm{LS}} = \mathbf{A}\mathbf{x}_{\mathrm{LS}} + \mathbf{v}_{\mathrm{LS}} \tag{1.9}$$

where $\mathbf{x}_{\mathrm{LS}} = \begin{bmatrix} x(0) & x(1) & \cdots & x(L-1) \end{bmatrix}^T$ is a $L \times 1$ vector containing the complex amplitudes over the entire range profile, $\mathbf{v}_{\mathrm{LS}} = \begin{bmatrix} v(0) & v(1) & \cdots & v(L+N-2) \end{bmatrix}^T$ is a $(L+N-1) \times 1$ vector of noise samples, and the matrix

$$\mathbf{A} = \begin{bmatrix} s_1 & 0 & \cdots & 0 \\ \vdots & s_1 & & \vdots \\ s_N & & \ddots & 0 \\ 0 & s_N & & s_1 \\ \vdots & & \ddots & \vdots \\ 0 & \cdots & 0 & s_N \end{bmatrix} \tag{1.10}$$

contains delay-shifted versions of the transmitted waveform. The Least-Squares estimate is formulated as

$$\hat{\mathbf{x}}_{\mathrm{LS}} = \left(\mathbf{A}^H \mathbf{A} \right)^{-1} \mathbf{A}\, \mathbf{y}_{\mathrm{LS}} \tag{1.11}$$

where $\hat{\mathbf{x}}_{\mathrm{LS}}$ is a $L \times 1$ vector containing the complex amplitude estimates of the entire range profile. The Least-Squares formulation will be referred to when presenting an over-sampled Least-Squares approach capable of super-resolution. Note the Least-Squares signal model in (1.9) does not account for scatterers just outside the processing window thus the estimate degrades significantly when a sizeable target is present within $N-1$ range cells of the processing window.

CHAPTER 2 DIMENSIONALITY ASPECTS OF ADAPTIVE PULSE COMPRESSION

2.1 Increased-Dimensionality APC and Least-Squares

2.1.1 Over-Sampled APC Signal Model and Filter

Increasing the dimensionality of the original APC algorithm, by over-sampling the received signal and transmitted waveform used for processing, yields an improvement in range resolution without increasing the bandwidth of the radar system. The received signal model is constructed by over-sampling, by a factor Λ, to obtain a super-resolved received signal model. Thus the received radar return at the ℓ^{th} range cell of a length-$L\Lambda$ over-sampled range profile can be defined as

$$\bar{y}(\ell) = \bar{\mathbf{x}}^T(\ell)\,\bar{\mathbf{s}} + v(\ell) \tag{2.1}$$

for $\ell = 0,\cdots, L\Lambda + N\Lambda - 2$, where $\bar{\mathbf{x}}(\ell) = \left[x(\ell) \quad x(\ell-1) \quad \cdots \quad x(\ell - N\Lambda + 1)\right]^T$ is the over-sampled portion of the range profile $\mathbf{x}(\ell)$ from (1.3), that the over-sampled waveform $\bar{\mathbf{s}} = \left[s_0 \quad s_1 \quad \cdots \quad s_{N\Lambda-1}\right]^T$ convolves with at delay ℓ, and $v(\ell)$ is again a sample of additive noise. Collecting $N\Lambda$ samples of the over-sampled received radar return signal, the system response model can be expressed as

$$\bar{\mathbf{y}}(\ell) = \bar{\mathbf{X}}^T(\ell)\,\bar{\mathbf{s}} + \bar{\mathbf{v}}(\ell) \tag{2.2}$$

where $\bar{\mathbf{y}}(\ell) = [\bar{y}(\ell) \quad \bar{y}(\ell+1) \quad \cdots \quad \bar{y}(\ell+N\Lambda-1)]^T$ is $N\Lambda$ contiguous samples of the received signal $\mathbf{y}(\ell)$ from (1.2) (at the higher sampling rate), the noise vector $\bar{\mathbf{v}}(\ell) = [v(\ell) \quad v(\ell+1) \quad \cdots \quad v(\ell+N\Lambda-1)]^T$, and the matrix

$$\begin{aligned}\bar{\mathbf{X}}(\ell) &= [\bar{\mathbf{x}}(\ell) \quad \bar{\mathbf{x}}(\ell+1) \quad \cdots \quad \bar{\mathbf{x}}(\ell+N\Lambda-1)] \\ &= \begin{bmatrix} x(\ell) & x(\ell+1) & \cdots & x(\ell+N\Lambda-1) \\ x(\ell-1) & x(\ell) & \cdots & x(\ell+N\Lambda-2) \\ \vdots & \vdots & \ddots & \vdots \\ x(\ell-N\Lambda+1) & \cdots & x(\ell-1) & x(\ell) \end{bmatrix}. \end{aligned} \tag{2.3}$$

This signal model will be utilized in minimizing the over-sampled APC cost function.

The over-sampled APC filter is obtained by minimizing a cost function that has the same form as the APC cost function, restated here for convenience

$$J(\ell) = E\left[\left|x(\ell) - \mathbf{w}^H(\ell)\mathbf{y}(\ell)\right|^2\right]. \tag{2.4}$$

However, the over-sampled APC cost function contains over-sampled versions of the APC filter $\mathbf{w}(\ell)$ and full-dimension signal model $\mathbf{y}(\ell)$. Thus, the over-sampled APC cost function is denoted

$$\bar{J}(\ell) = E\left[\left|x(\ell) - \bar{\mathbf{w}}^H(\ell)\bar{\mathbf{y}}(\ell)\right|^2\right] \tag{2.5}$$

where $\bar{\mathbf{y}}(\ell)$ is the over-sampled (by Λ) system response model from (2.2) and $\bar{\mathbf{w}}(\ell) = [w_0 \quad w_1 \quad \cdots \quad w_{N\Lambda-1}]^T$ is the over-sampled pulse compression filter. The cost function from (2.5) is minimized in a manner identical to the APC cost function resulting in an over-sampled version of the APC filter expressed as

$$\bar{\mathbf{w}}(\ell) = \rho(\ell)\left(\bar{\mathbf{C}}(\ell) + \bar{\mathbf{R}}\right)^{-1}\bar{\mathbf{s}} \tag{2.6}$$

for $\ell = 0,1,\cdots, L\Lambda - 1$, where $\rho(\ell) = E\left[\left|x(\ell)\right|^2\right]$ is the expected power of $x(\ell)$, $\overline{\mathbf{R}} = E\left[\bar{\mathbf{v}}(\ell)\bar{\mathbf{v}}^H(\ell)\right]$ is an over-sampled noise covariance matrix, $\bar{\mathbf{s}}$ represents the over-sampled waveform, and the over-sampled signal correlation matrix $\overline{\mathbf{C}}(\ell)$ is

$$\overline{\mathbf{C}}(\ell) = \sum_{n=-N\Lambda+1}^{N\Lambda-1} \rho(\ell + n)\,\bar{\mathbf{s}}_n \bar{\mathbf{s}}_n^H \tag{2.7}$$

where $\bar{\mathbf{s}}_n$ represents a delay-shifted version of the over-sampled waveform with the remainder zero-filled, *e.g.* $\bar{\mathbf{s}}_1 = \begin{bmatrix} 0 & s_0 & \cdots & s_{N\Lambda-2} \end{bmatrix}^T$ and $\bar{\mathbf{s}}_{-1} = \begin{bmatrix} s_1 & \cdots & s_{N\Lambda-1} & 0 \end{bmatrix}^T$.

2.1.2 Over-Sampled Least-Squares Signal Model and Filter

The Least-Squares algorithm can also be used to achieve super-resolution [16] when the received signal and transmitted waveform are over-sampled. Over-sampling the Least-Squares model in (1.9) yields

$$\bar{\mathbf{y}}_{\mathrm{LS}} = \overline{\mathbf{A}}\bar{\mathbf{x}}_{\mathrm{LS}} + \bar{\mathbf{v}}_{\mathrm{LS}} \tag{2.8}$$

where $\bar{\mathbf{x}}_{\mathrm{LS}} = \begin{bmatrix} x(0) & x(1) & \cdots & x(L\Lambda - 1) \end{bmatrix}^T$ is a $L\Lambda \times 1$ vector containing the complex amplitudes over the entire range profile, the over-sampled noise vector $\bar{\mathbf{v}}_{\mathrm{LS}} = \begin{bmatrix} v(0) & v(1) & \cdots & v(L\Lambda + N\Lambda - 2) \end{bmatrix}^T$ is now $(L\Lambda + N\Lambda - 1) \times 1$, and the over-sampled matrix

$$\overline{\mathbf{A}} = \begin{bmatrix} s_1 & 0 & \cdots & 0 \\ \vdots & s_1 & & \vdots \\ s_{N\Delta} & & \ddots & 0 \\ 0 & s_{N\Lambda} & & s_1 \\ \vdots & & \ddots & \vdots \\ 0 & \cdots & 0 & s_{N\Lambda} \end{bmatrix} \tag{2.9}$$

contains delay-shifted versions of the over-sampled transmit waveform $\overline{\mathbf{s}}$.

The over-sampled Least-Squares formulation used in this thesis based on the over-sampled signal model above is denoted

$$\hat{\overline{\mathbf{x}}}_{\mathrm{LS}} = \left(\overline{\mathbf{A}}^H \overline{\mathbf{A}}\right)^{-1} \overline{\mathbf{A}}\, \overline{\mathbf{y}}_{\mathrm{LS}} \tag{2.10}$$

where $\hat{\overline{\mathbf{x}}}_{\mathrm{LS}}$ is now a $L\Lambda \times 1$ vector containing the complex amplitude estimates of the entire over-sampled range profile.

2.2 Reduced-Dimensionality Signal Models

Reducing the dimensionality of APC yields a new algorithm which can be utilized to lower computational complexity without sacrificing significant performance. The reduced-dimension signal models are formed by subdividing the full-dimension APC signal model in (1.1). This is accomplished by segregating the N received signal samples of $\mathbf{y}(\ell)$ into M segments of length $N/M = K$ using either contiguous blocking or decimation. The following details the particular form of the reduced-dimension signal models for the two embodiments of Fast APC.

The decimated model of the received signal is constructed by decimating the full-dimension received signal from (1.3) as

$$\widetilde{\mathbf{y}}_{D,m}(\ell)=\begin{bmatrix} y(\ell+m) & y(\ell+M+m) & \cdots & y(\ell+N-2M+m) & y(\ell+N-M+m)\end{bmatrix}^T \tag{2.11}$$

for $m=0,1,\cdots,M-1$. Thus, the matrix $\mathbf{X}(\ell)$ from (3) is partitioned into M sub-matrices of dimension $N\times K$ as

$$\widetilde{\mathbf{X}}_{D,m}(\ell)=\begin{bmatrix} \mathbf{x}(\ell+m) & \mathbf{x}(\ell+M+m) & \cdots & \mathbf{x}(\ell+N-2M+m) & \mathbf{x}(\ell+N-M+m)\end{bmatrix} \tag{2.13}$$

for $m=0,1,\cdots,M-1$. The noise vector $\mathbf{v}(\ell)$ is likewise segmented as

$$\widetilde{\mathbf{v}}_{D,m}(\ell)=\begin{bmatrix} v(\ell+m) & v(\ell+M+m) & \cdots & v(\ell+N-2M+m) & v(\ell+N-M+m)\end{bmatrix}^T \tag{2.14}$$

thus producing the decimated received signal model

$$\widetilde{\mathbf{y}}_{D,m}(\ell)=\widetilde{\mathbf{X}}_{D,m}^T(\ell)\mathbf{s}+\widetilde{\mathbf{v}}_{D,m}(\ell). \tag{2.15}$$

In a similar manner the contiguous blocking model of the received signal is constructed by segmenting the full-dimension received signal from (1.1) as

$$\widetilde{\mathbf{y}}_{C,m}(\ell)=\begin{bmatrix} y(\ell+Km) & y(\ell+Km+1) & \cdots & y(\ell+Km+K-2) & y(\ell+Km+K-1)\end{bmatrix}^T \tag{2.16}$$

for $m=0,1,\cdots,M-1$. As such, the matrix $\mathbf{X}(\ell)$ from (1.3) is partitioned into M sub-matrices of dimension $N\times K$ as

$$\widetilde{\mathbf{X}}_{C,m}(\ell)=\left[\mathbf{x}(\ell+Km)\quad \mathbf{x}(\ell+Km+1)\quad \cdots\quad \mathbf{x}(\ell+Km+K-2)\quad \mathbf{x}(\ell+Km+K-1)\right] \tag{2.17}$$

for $m=0,1,\cdots,M-1$. The contiguously blocked noise vector is similarly segmented as

$$\widetilde{\mathbf{v}}_{C,m}(\ell)=\left[v(\ell+Km)\quad v(\ell+Km+1)\quad \cdots\quad v(\ell+Km+K-2)\quad v(\ell+Km+K-1)\right]^T \tag{2.18}$$

thereby yielding the contiguously blocked received signal model

$$\widetilde{\mathbf{y}}_{C,m}(\ell)=\widetilde{\mathbf{X}}_{C,m}^T(\ell)\mathbf{s}+\widetilde{\mathbf{v}}_{C,m}(\ell). \tag{2.19}$$

The two reduced-dimension received signal models of (2.15) and (2.19) will be employed to derive two particular embodiments of the Fast Adaptive Pulse Compression (FAPC) algorithm.

2.3 Derivation of Fast APC

The Fast APC cost function is formed by approximating the APC cost function in (1.5) as the summation of *M* segments denoted

$$\widetilde{J}(\ell)=\sum_{m=1}^{M-1}E\left[\left|\frac{1}{M}x(\ell)-\widetilde{\mathbf{w}}_m^H(\ell)\widetilde{\mathbf{y}}_m(\ell)\right|^2\right] \tag{2.20}$$

where $\widetilde{\mathbf{w}}_m(\ell)$ is the m^{th} *K*-length segment (according to either decimation or contiguous blocking) of the *N*-length piecewise MMSE filter, denoted $\widetilde{\mathbf{w}}(\ell)$, and $\widetilde{\mathbf{y}}_m(\ell)$ is the m^{th} *K*-length segment of the *N*-length $\mathbf{y}(\ell)$ also according to either

decimation or contiguous blocking. Minimization of the piecewise MMSE cost function of (2.20) yields the piecewise MMSE pulse compression filter $\widetilde{\mathbf{w}}(\ell)$, which approximates the filter formed using the full-dimension algorithm. The m^{th} K-length segment of $\widetilde{\mathbf{w}}(\ell)$ is denoted as

$$\widetilde{\mathbf{w}}_m(\ell) = \left(E\left[\widetilde{\mathbf{y}}_m(\ell)\,\widetilde{\mathbf{y}}_m^H(\ell)\right]\right)^{-1} E\left[\frac{1}{M}\widetilde{\mathbf{y}}_m(\ell)\,x^*(\ell)\right] \tag{2.21}$$

for $m = 0,1,\cdots,M-1$, where $(\bullet)^*$ is the complex conjugate operation. The following details the particular form realized by (2.21) when employing decimation and contiguous blocking, respectively.

2.3.1 Decimation FAPC

For the decimation embodiment of Fast APC the m^{th} filter segment $\widetilde{\mathbf{w}}_m(\ell)$ from (2.21) is given by

$$\widetilde{\mathbf{w}}_{D,m}(\ell) = \left[w_m \quad w_{M+m} \quad w_{2M+m} \quad \cdots \quad w_{N-3M+m} \quad w_{N-2M+m} \quad w_{N-M+m}\right]^T. \tag{2.22}$$

For example, with $N = 12$ and $M = 3$ so that $K = \frac{12}{3} = 4$, the Fast APC filter is

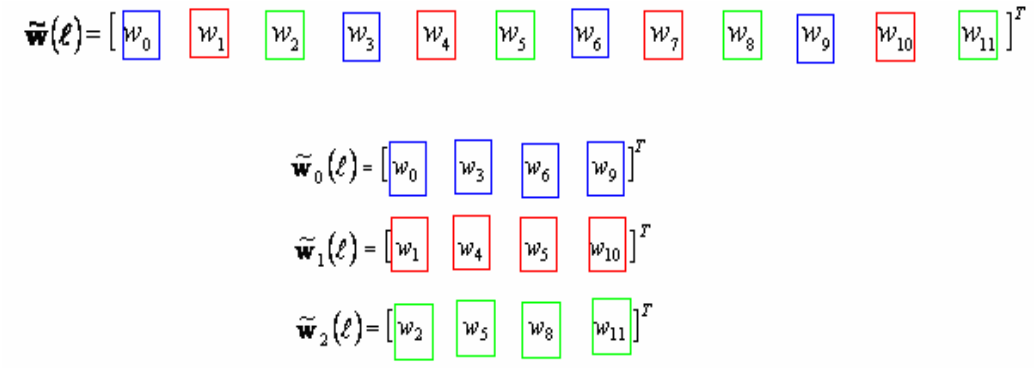

Figure 2.1 Example Showing Decimation FAPC Coefficient Allocation

where $\tilde{\mathbf{w}}_m(\ell)$ is the m^{th} decimated segment of the filter. This filter is found by substituting the decimated received signal model $\tilde{\mathbf{y}}_{D,m}(\ell)$ from (2.15) into (2.21) and assuming that the range cells are, in general, uncorrelated with one another and also uncorrelated with the noise, the decimated filter segments are obtained as

$$\tilde{\mathbf{w}}_{D,m}(\ell) = \frac{1}{M}\rho(\ell)\left(\tilde{\mathbf{C}}_{D,m}(\ell) + \tilde{\mathbf{R}}_{D,m}\right)^{-1}\tilde{\mathbf{d}}_{m,0} \tag{2.23}$$

where $\rho(\ell) = E\left[\,|x(\ell)|^2\,\right]$ is the expected power of $x(\ell)$, $\tilde{\mathbf{R}}_{D,m} = E\left[\tilde{\mathbf{v}}_{D,m}(\ell)\tilde{\mathbf{v}}_{D,m}^H(\ell)\right]$ is the $K \times K$ decimated noise covariance matrix based on (2.14), and $\tilde{\mathbf{d}}_{m,0}$ is the $K \times 1$ decimated waveform vector

$$\tilde{\mathbf{d}}_{m,0} = \left[s_m \quad s_{M+m} \quad s_{2M+m} \quad \cdots \quad s_{N-M+m}\right]^T. \tag{2.24}$$

The $K \times K$ decimated signal correlation matrix $\tilde{\mathbf{C}}_{D,m}(\ell)$ is constructed as

$$\tilde{\mathbf{C}}_{D,m}(\ell) = \sum_{i=0}^{M-1}\sum_{k=-K+1}^{K-1}\rho(\ell + Mk - i + m)\,\tilde{\mathbf{d}}_{i,k}\,\tilde{\mathbf{d}}_{i,k}^H \tag{2.25}$$

where $\widetilde{\mathbf{d}}_{i,k}$ is the vector $\widetilde{\mathbf{d}}_{i,0}$ shifted by k samples and the remainder zero-filled. Thus, for $k > 0$

$$\widetilde{\mathbf{d}}_{m,k} = \begin{bmatrix} \mathbf{0}_{1\times k} & s_m & s_{M+m} & \cdots & s_{N-M(k+1)+m} \end{bmatrix}^T \tag{2.26}$$

and for $k < 0$

$$\widetilde{\mathbf{d}}_{m,k} = \begin{bmatrix} s_{kM+m} & \cdots & s_{N-2M+m} & s_{N-M+m} & \mathbf{0}_{1\times|k|} \end{bmatrix}^T . \tag{2.27}$$

Fig. 2.2 illustrates a simple example, with $N = 4$ and $M = 2$, that displays how utilization of the decimated signal model results in a sampling of the full-dimension signal correlation matrix $\mathbf{C}(\ell)$ from (1.8) to form the decimation-based reduced-dimension signal correlation matrices $\widetilde{\mathbf{C}}_{D,0}(\ell)$ and $\widetilde{\mathbf{C}}_{D,1}(\ell)$ from (2.25). In Fig.2.2, the terms in the ovals, namely $c_{1,1}(\ell)$, $c_{3,1}(\ell)$, $c_{1,3}(\ell)$, and $c_{3,3}(\ell)$, are the elements of $\mathbf{C}(\ell)$ that constitute $\widetilde{\mathbf{C}}_{D,0}(\ell)$, while the terms $c_{2,2}(\ell)$, $c_{4,2}(\ell)$, $c_{2,4}(\ell)$, and $c_{4,4}(\ell)$ in the boxes comprise $\widetilde{\mathbf{C}}_{D,1}(\ell)$. Also, note that upon incrementing the range index from ℓ to $\ell+1$, the matrix $\widetilde{\mathbf{C}}_{D,1}(\ell)$ becomes $\widetilde{\mathbf{C}}_{D,0}(\ell+1)$. In general, this means that only one new reduced-dimension signal correlation matrix needs to be determined for the $(\ell+1)^{th}$ range cell index as the other $M-1$ matrices are already available at the ℓ^{th} range cell. This property of the decimated filter will be exploited to obtain an efficient implementation structure.

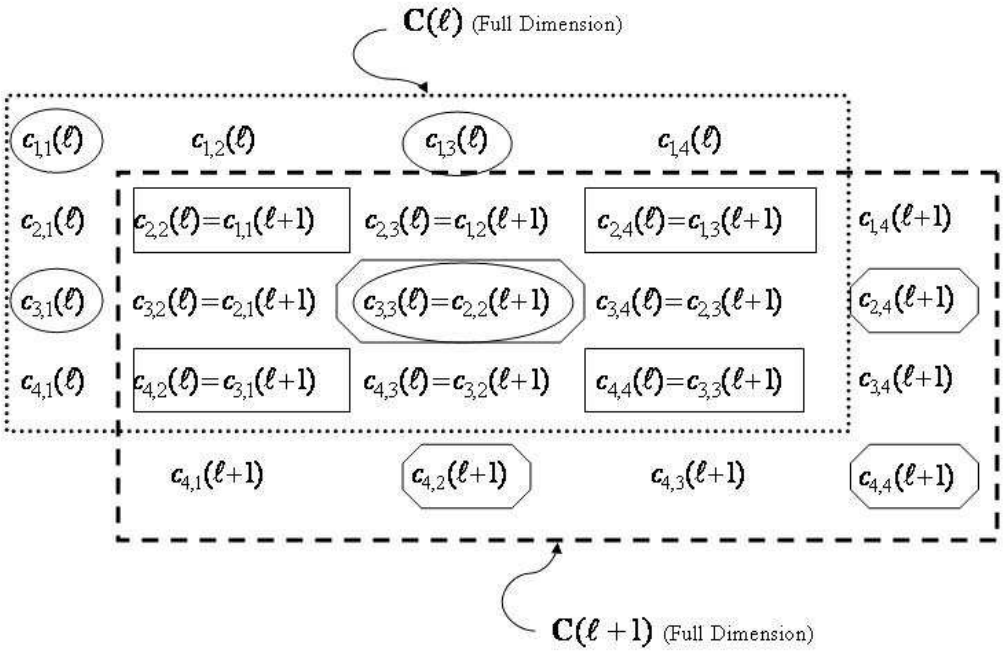

Figure 2.2 Comparison of Full-Dimension and Reduced-Dimension Signal Correlation Matrices (Decimation FAPC)

2.3.2 Contiguous FAPC

The second embodiment of FAPC uses contiguous blocking in place of decimation. For the blocking approach, the segments of the piecewise MMSE filter from (2.21) are given by

$$\tilde{\mathbf{w}}_{D,m}(\ell)=\begin{bmatrix} w_{Km} & w_{Km+1} & w_{Km+2} & \cdots & w_{Km+K-3} & w_{Km+K-2} & w_{Km+K-1} \end{bmatrix}^T \quad (2.28)$$

for $m = 0,1,\cdots,M-1$. For example, given $N=12$, $M=3$ so that $K=\frac{12}{3}=4$ yields

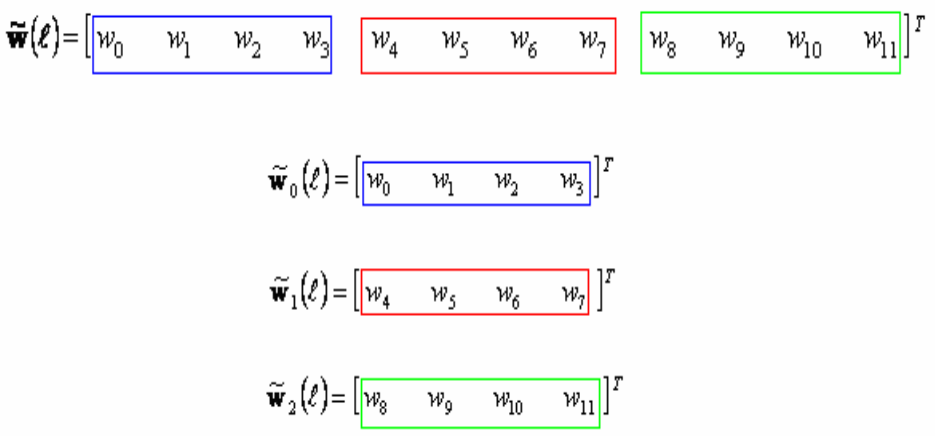

Figure 2.1 Example Showing Contiguous FAPC Coefficient Allocation

where $\tilde{\mathbf{w}}_m(\ell)$ is the m^{th} blocked segment of the filter $\tilde{\mathbf{w}}(\ell)$. The filter segments are obtained by inserting the contiguously blocked received signal model $\tilde{\mathbf{y}}_{C,m}(\ell)$, from (2.19), into (2.21). The blocked filter segments can be obtained in a similar manner as the decimation embodiment of Fast APC by again assuming that the range cells are, in general, uncorrelated with one another and also uncorrelated with the noise. For this case, we express the K-length shifted versions of the transmit waveform segments using the column vectors of the $K \times (N+K-1)$ matrix

$$\begin{bmatrix} s_{N-1} & s_{N-2} & \cdots & s_0 & 0 & \cdots & 0 & 0 \\ 0 & s_{N-1} & \cdots & s_1 & s_0 & & \vdots & \vdots \\ \vdots & 0 & \ddots & s_2 & s_1 & \ddots & 0 & \vdots \\ \vdots & \vdots & & \vdots & \vdots & \ddots & s_0 & 0 \\ 0 & 0 & & s_{K-1} & s_{K-2} & \cdots & s_1 & s_0 \end{bmatrix} = \begin{bmatrix} \tilde{\mathbf{b}}_{-N+1} & \tilde{\mathbf{b}}_{-N+2} & \cdots & \tilde{\mathbf{b}}_0 & \tilde{\mathbf{b}}_1 & \cdots & \tilde{\mathbf{b}}_{K-2} & \tilde{\mathbf{b}}_{K-1} \end{bmatrix} \tag{2.29}$$

Thus, the contiguous FAPC filter is denoted

$$\widetilde{\mathbf{w}}_{C,m}(\ell) = \frac{1}{M}\rho(\ell)\left(\widetilde{\mathbf{C}}_{C,m}(\ell) + \widetilde{\mathbf{R}}_{C,m}\right)^{-1}\widetilde{\mathbf{b}}_{\beta(m)} \tag{2.30}$$

for $m = 0,1,\cdots,M-1$, where $\rho(\ell) = E\left[\,|x(\ell)|^2\,\right]$ is the expected power of $x(\ell)$, $\widetilde{\mathbf{R}}_{C,m} = E\left[\widetilde{\mathbf{v}}_{C,m}(\ell)\widetilde{\mathbf{v}}_{C,m}^{H}(\ell)\right]$ is the $K \times K$ blocked noise covariance matrix based on (2.18), and the $K \times K$ blocked signal correlation matrix $\widetilde{\mathbf{C}}_{C,m}(\ell)$ is expressed as

$$\widetilde{\mathbf{C}}_{C,m}(\ell) = \sum_{k=-N+1}^{K-1}\rho(\ell + k + Km)\,\widetilde{\mathbf{b}}_k\,\widetilde{\mathbf{b}}_k^{H}\,. \tag{2.31}$$

In equation (2.30) the subscript $\beta(m) = -Km$ such that $\widetilde{\mathbf{b}}_{\beta(m)}$ is the $(m+1)^{th}$ length-K contiguous segment of the transmit waveform $\mathbf{s}$.

Fig. 2.4 illustrates the simple example with $N = 4$ and $M = 2$ in which the contiguous signal model results in a sampling of the full-dimension matrix $\mathbf{C}(\ell)$ from (1.8) to form the contiguous-based reduced-dimension signal correlation matrices $\widetilde{\mathbf{C}}_{C,0}(\ell)$ and $\widetilde{\mathbf{C}}_{C,1}(\ell)$ from (2.31). In Fig. 2.4, the terms in the upper-left box, namely $c_{1,1}(\ell)$, $c_{1,2}(\ell)$, $c_{2,1}(\ell)$, and $c_{2,2}(\ell)$, constitute $\widetilde{\mathbf{C}}_{C,0}(\ell)$, while the terms $c_{3,3}(\ell)$, $c_{3,4}(\ell)$, $c_{4,3}(\ell)$, and $c_{4,4}(\ell)$ in the lower-right box comprise $\widetilde{\mathbf{C}}_{C,1}(\ell)$. Incrementing the range index by 1 results in the upper-left octagon containing $\widetilde{\mathbf{C}}_{C,0}(\ell+1)$ and the lower-right octagon containing $\widetilde{\mathbf{C}}_{C,1}(\ell+1)$. Furthermore, note that if the range index were incremented from ℓ to $\ell + K$,

where $K = N/M$ ($K = 2$ in this example), then $\tilde{\mathbf{C}}_{C,1}(\ell)$ becomes $\tilde{\mathbf{C}}_{C,0}(\ell + K)$. In general, this means that the reduced-dimension signal correlation matrices can be stored in memory to be reused after a shift of K range cell indices. This property of the contiguously-blocked filter will be utilized to obtain an efficient implementation structure.

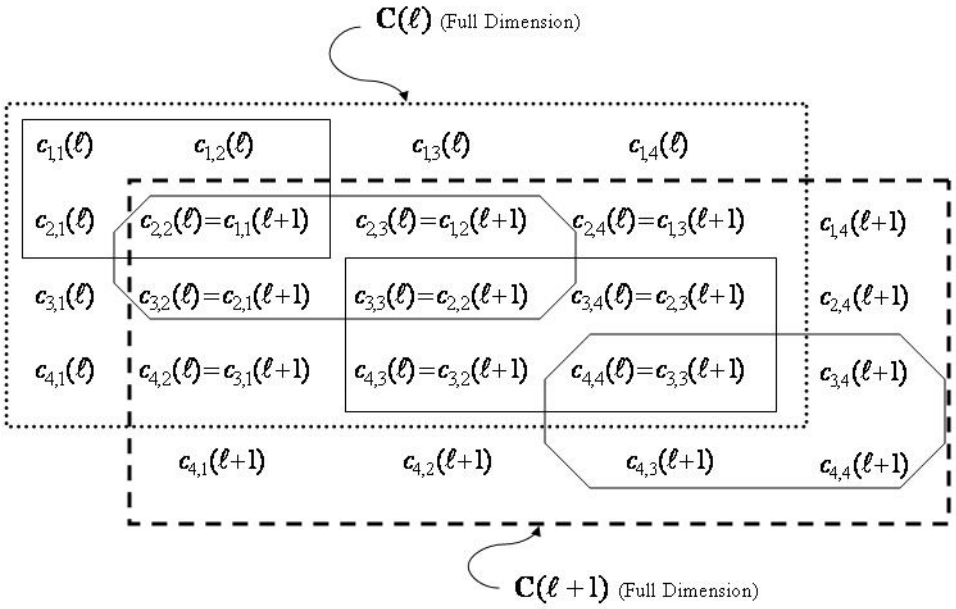

Figure 2.4 Comparison of Full-Dimension and Reduced-Dimension Signal Correlation Matrices (Contiguous FAPC)

2.4 Analysis of Fast APC Filter

The APC filter has been shown to reduce to an approximation of the normalized matched filter when a solitary point target in white noise is present [12]. This chapter will explore an analytical approximation of the contiguous FAPC pulse compression filter for the same scenario. The goal here is to analytically examine the mismatch loss characteristics of the Fast APC filter when a single small target is present.

First, examine the m^{th} signal correlation matrix from (2.31) for a range cell containing a single point target in white noise approximated by

$$\widetilde{\mathbf{C}}_{C,m}(\ell) = \rho(\ell)\widetilde{\mathbf{b}}_{\beta(m)}\widetilde{\mathbf{b}}_{\beta(m)}^{H} + \psi \sum_{\substack{k=-N+1 \\ k\neq\beta(m)}}^{K-1} \widetilde{\mathbf{b}}_k \widetilde{\mathbf{b}}_k^{H} \tag{2.32}$$

where ψ is the maximum *a priori* power estimate in the surrounding range cells and $\beta(m) = -Km$. The filter segments can then be found by inserting (2.32) into (2.30) resulting in

$$\widetilde{\mathbf{w}}_{C,m}(\ell) = \frac{\rho(\ell)}{M}\left(\rho(\ell)\widetilde{\mathbf{b}}_{\beta(m)}\widetilde{\mathbf{b}}_{\beta(m)}^{H} + \psi \sum_{\substack{k=-N+1 \\ k\neq\beta(m)}}^{K-1} \widetilde{\mathbf{b}}_k \widetilde{\mathbf{b}}_k^{H} + \widetilde{\mathbf{R}}_{C,m} \right)^{-1} \widetilde{\mathbf{s}}_{\beta(m)} \ . \tag{2.33}$$

The reduced-dimension correlation matrix from (2.32) can be rewritten in matrix form as

$$\widetilde{\mathbf{B}}\mathbf{Q}\widetilde{\mathbf{B}}^{H} = \rho(\ell)\widetilde{\mathbf{b}}_{\beta(m)}\widetilde{\mathbf{b}}_{\beta(m)}^{H} + \psi \sum_{\substack{k=-N+1 \\ k\neq\beta(m)}}^{K-1} \widetilde{\mathbf{b}}_k \widetilde{\mathbf{b}}_k^{H} \tag{2.34}$$

where

$$\begin{bmatrix} s_{N-1} & s_{N-2} & \cdots & s_0 & 0 & \cdots & 0 & 0 \\ 0 & s_{N-1} & \cdots & s_1 & s_0 & & \vdots & \vdots \\ \vdots & 0 & \ddots & s_2 & s_1 & \ddots & 0 & \vdots \\ \vdots & \vdots & & \vdots & \vdots & \ddots & s_0 & 0 \\ 0 & 0 & & s_{K-1} & s_{K-2} & \cdots & s_1 & s_0 \end{bmatrix}$$
$$= \widetilde{\mathbf{B}} = \begin{bmatrix} \widetilde{\mathbf{b}}_{-N+1} & \widetilde{\mathbf{b}}_{-N+2} & \cdots & \widetilde{\mathbf{b}}_0 & \widetilde{\mathbf{b}}_1 & \cdots & \widetilde{\mathbf{b}}_{K-2} & \widetilde{\mathbf{b}}_{K-1} \end{bmatrix} \tag{2.35}$$

and $\mathbf{Q}$ is the diagonal matrix

$$diag\{\mathbf{Q}\} = \begin{bmatrix} \psi & \cdots & \psi & \rho(\ell) & \psi & \cdots & \psi \end{bmatrix} \tag{2.36}$$

with $\rho(\ell)$ corresponding to the column $\widetilde{\mathbf{b}}_{\beta(m)}$ in $\widetilde{\mathbf{B}}$.

The following shows how the inverted term in (2.33) can be found using the matrix inversion lemma [18]. Utilizing the lemma along with (2.34) the inverse at the ℓ^{th} range cell (containing the point target) can be denoted

$$\left(\sigma_v^2\mathbf{I} + \widetilde{\mathbf{B}}\mathbf{Q}\widetilde{\mathbf{B}}^H\right)^{-1} = \frac{1}{\sigma_v^2}\mathbf{I} - \frac{1}{\sigma_v^2}\widetilde{\mathbf{B}}\left(\mathbf{Q}^{-1} + \frac{1}{\sigma_v^2}\widetilde{\mathbf{B}}^H\widetilde{\mathbf{B}}\right)^{-1}\frac{1}{\sigma_v^2}\widetilde{\mathbf{B}}^H \tag{2.37}$$

where σ_v^2 is the noise power. Assuming the waveform is orthogonal to sample-shifted versions of itself, *i.e.* approximating a waveform with low autocorrelation sidelobes, the term to be inverted on the right side of (2.37) can be expressed as a diagonal matrix with

$$diag\left\{\mathbf{Q}^{-1} + \frac{1}{\sigma_v^2}\widetilde{\mathbf{B}}^H\widetilde{\mathbf{B}}\right\} \approx$$
$$\left[\frac{\psi+\sigma_v^2}{\psi\sigma_v^2} \quad \frac{2\psi+\sigma_v^2}{\psi\sigma_v^2} \quad \cdots \quad \frac{K\psi+\sigma_v^2}{\psi\sigma_v^2} \quad \cdots \quad \frac{K\psi+\sigma_v^2}{\psi\sigma_v^2} \cdots\right. \tag{2.38}$$
$$\left. \cdots \frac{K\rho(\ell)+\sigma_v^2}{\rho(\ell)\sigma_v^2} \quad \frac{(K-1)\psi+\sigma_v^2}{\psi\sigma_v^2} \quad \frac{(K-2)\psi+\sigma_v^2}{\psi\sigma_v^2} \quad \cdots \quad \frac{\psi+\sigma_v^2}{\psi\sigma_v^2}\right].$$

Combining (2.37) and (2.38) yields

$$\left(\sigma_v^2\mathbf{I}+\widetilde{\mathbf{B}}\mathbf{Q}\widetilde{\mathbf{B}}^H\right)^{-1}\approx \frac{1}{\sigma_v^2}\mathbf{I}-\frac{\rho(\ell)}{\sigma_v^2\left(\sigma_v^2+K\rho(\ell)\right)}\widetilde{\mathbf{b}}_{\beta(m)}\widetilde{\mathbf{b}}_{\beta(m)}^H+\sum_{\substack{k=-N+1\\k\neq\beta(m)}}^{K-1}\frac{\psi}{\sigma_v^2\left(\sigma_v^2+f(k)\psi\right)}\widetilde{\mathbf{b}}_k\widetilde{\mathbf{b}}_k^H \quad (2.39)$$

where $f(k)$ is a function containing values between 1 and K corresponding to the elements shown in (2.38).

Inserting the result from (2.39) into the filter equation in (2.33) results in the Fast APC filter segments

$$\widetilde{\mathbf{w}}_{C,m}(\ell)\approx\frac{1}{M}\left(\frac{\rho(\ell)}{\sigma_v^2+K\rho(\ell)}\widetilde{\mathbf{b}}_{\beta(m)}-\sum_{\substack{k=-N+1\\k\neq\beta(m)}}^{K-1}\frac{\psi\varphi\rho(\ell)}{\sigma_v^2\left(\sigma_v^2+f(k)\psi\right)}\widetilde{\mathbf{b}}_k\right) \quad (2.40)$$

where $\varphi\rho(\ell)$ is the maximum sidelobe level in the surrounding range cells. Assuming the sidelobe level and power estimates in surrounding range cells are relatively small the second term in (2.40) can be neglected thus the pulse compression filter for the range cell containing the large target can be approximated as

$$\widetilde{\mathbf{w}}_{C,m}(\ell)\approx\frac{\frac{1}{M}\rho(\ell)}{\sigma_v^2+K\rho(\ell)}\widetilde{\mathbf{b}}_{\beta(m)}\ . \quad (2.41)$$

Upon inspection of (2.41) it is evident that the N-length piecewise contiguous FAPC filter $\widetilde{\mathbf{w}}(\ell)$ can be expressed as

$$\widetilde{\mathbf{w}}(\ell)\approx\frac{\frac{1}{M}\rho(\ell)}{\sigma_v^2+K\rho(\ell)}\left[\widetilde{\mathbf{b}}_{\beta(0)}^T\quad\widetilde{\mathbf{b}}_{\beta(1)}^T\quad\cdots\quad\widetilde{\mathbf{b}}_{\beta(M-1)}^T\right]^T. \quad (2.42)$$

Examining (2.42) yields a simplified version of the filter denoted

$$\tilde{\mathbf{w}}(\ell) \approx \frac{\frac{1}{M}\rho(\ell)}{\sigma_v^2 + \frac{N}{M}\rho(\ell)}\mathbf{s} \ . \tag{2.43}$$

Thus, the contiguous Fast APC filter for a single point target in noise is approximately equal to a scaled version of the normalized matched filter. When compared to the analytical approximation of the APC filter from [12] given as

$$\mathbf{w}(\ell) \approx \frac{\rho(\ell)}{\sigma_v^2 + N\rho(\ell)}\mathbf{s} \tag{2.44}$$

the Fast APC filter in (2.43) is less sensitive to the power estimate *i.e.* the FAPC filter requires higher SNR to approximate the normalized matched filter than the APC version in (2.44). For this reason, it is suspected and has been observed that the contiguous Fast APC exhibits mismatch loss, especially in the case of a solitary small RCS scatterer. To alleviate this loss the piecewise contiguous filter can be normalized such that practically no mismatch loss is present in the case of a solitary point scatterer. This is achieved by dividing the filter at each range cell by the inner product of the filter and waveform as

$$\tilde{\mathbf{w}}(\ell) = \frac{\tilde{\mathbf{w}}(\ell)}{\tilde{\mathbf{w}}^H(\ell)\mathbf{s}} \ . \tag{2.45}$$

The technique in (2.45) almost completely mitigates mismatch loss for the case of a single small target and has been observed to improve estimation error in sparse channels. The scaled filter in (2.45) exhibits degraded sidelobe suppression in dense channels but is much more robust to small scatterers than the unaltered Fast

APC filter which tends to over-suppress as the segmentation factor M becomes large, resulting in suppression of small targets. The analysis of constraints such as that in (2.45) has been left as future work.

CHAPTER 3 IMPLEMENTATION ISSUES

3.1 General Implementation

FAPC and over-sampled APC utilize the reiterative MMSE structure seen in [12] whereby the range cell estimates are employed to determine the adaptive filter for each individual range delay which then yields an updated estimate for the particular range cell. The normalized matched filter can be used as the first stage to obtain an initial range profile estimate, which is required in order to compute the pulse compression filter for each range cell. The matched filter is then replaced at the second stage by the unique length-N adaptive filter for each individual range cell. At each successive stage the range profile estimate from the previous stage is employed as *a priori* information to determine power estimates required to obtain the current adaptive filters.

It has been observed in [12] that when the squared magnitude of the complex amplitude estimate $\rho(\ell) = |x(\ell)|^2$ is used the APC algorithm may not always converge to a solution. Thus, the strategy employed in [12] has been utilized in this thesis to compute the power estimates for over-sampled APC and Fast APC as

$$\rho(\ell) = |x(\ell)|^{\mu} \tag{3.1}$$

where $\mu = 1.7,\ 1.3,\ 1.1$ for the first three adaptive stages, respectively. Based on simulations, two to three adaptive stages have been found to sufficiently suppress the range sidelobes into the noise.

3.2 Increased Dimensionality Issues

The over-sampled versions of Least-Squares and APC yield matrices that contain elements from the over-sampled transmit waveform. Over-sampling the transmitted waveform yields less delay between successive samples thus consecutive samples may become similar, especially when a discrete time waveform is used. The similarity between samples in the over-sampled APC and Least-Squares filter matrices may lead to moderate ill-conditioning. This effect is evident in Figs. 3.1 and 3.2 which compare the Eigenvalues of the matrix products $\mathbf{A}^H\mathbf{A}$ and $\overline{\mathbf{A}}^H\overline{\mathbf{A}}$ found in the nominal and over-sampled Least-Squares formulations, respectively. The transmit waveform, a P3 code [3] with a nominal length of $N = 20$, was over-sampled by 5 to produce the values in Fig. 3.2. Adaptive diagonal loading was used in [16] to alleviate ill-conditioning for an over-sampled version of Least-Squares. In this thesis traditional diagonal loading will be utilized to reduce the effects and is applied to the APC and Least-Square filters from (2.6) and (2.10), respectively, by adding a weighted identity matrix as

$$\overline{\mathbf{w}}(\ell) = \rho(\ell)\left(\overline{\mathbf{C}}(\ell) + \gamma\,\overline{\mathbf{R}}\right)^{-1}\overline{\mathbf{s}} \tag{3.2}$$

$$\overline{\mathbf{x}}_{\mathrm{LS}} = \left(\overline{\mathbf{A}}^H\overline{\mathbf{A}} + \delta\,\mathbf{I}\right)^{-1}\overline{\mathbf{A}}\,\overline{\mathbf{y}}_{\mathrm{LS}} \tag{3.3}$$

where γ and δ are the loading factors for the over-sampled versions of APC and Least-Squares, respectively. In (3.2) the over-sampled APC noise covariance matrix $\overline{\mathbf{R}}$ is assumed to be a weighted identity matrix, *i.e.* the noise is white. In the general case of colored noise the loading can be employed as

$$\overline{\mathbf{w}}(\ell) = \rho(\ell)\left(\overline{\mathbf{C}}(\ell) + \overline{\mathbf{R}} + \gamma \mathbf{I}\right)^{-1}\overline{\mathbf{s}}\,. \tag{3.4}$$

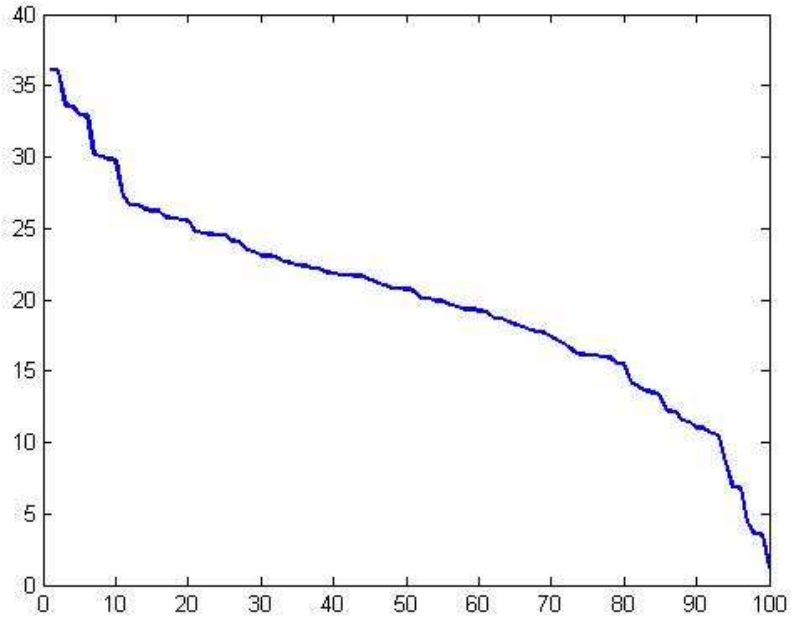

Figure 3.1 Eigenvalues for Least-Squares at Nominal Sampling Rate with length $N = 20$ Waveform (length $L = 100$ Range Profile)

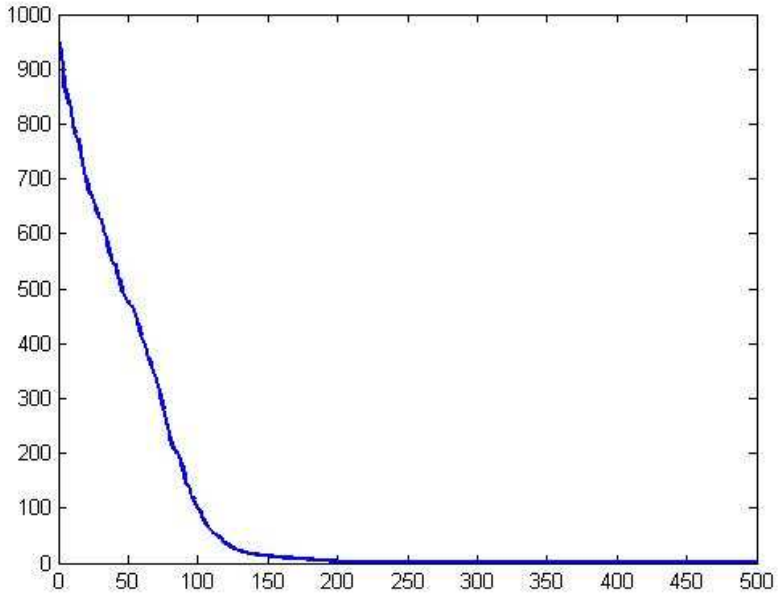

Figure 3.2 Eigenvalues for Least-Squares at 5*X* the Nominal Sampling Rate with length $N = 20 \times 5 = 100$ Waveform (length $L = 100 \times 5 = 500$ Range Profile)

3.3 Reduced Dimensionality Issues

3.3.1 Efficient Implementation of APC

The full-dimension APC algorithm requires computing a $N \times N$ (where N is the length of the transmit waveform) matrix inverse at each range cell which results in a relatively high computational complexity, on the order of N^3 complex multiplies per range cell. However, the structure of the signal correlation matrices at successive range cells allows a fast update technique [12], based on the matrix inversion lemma [18], to be used reducing the computational cost of the inverse to $O\left(N^2\right)$. Note that the matrix inversion lemma will be used here to determine a rank-3 matrix update as opposed to the previous chapter where the lemma was

used to compute a full-rank update for analysis purposes. The following describes the procedure used in [12] to perform the fast matrix update.

The full-dimension APC signal correlation matrices are structured such that the signal correlation matrix at the $(\ell+1)^{th}$ range cell is related to the signal correlation matrix at the ℓ^{th} range cell as follows

$$\mathbf{C}(\ell)+\mathbf{R}=\begin{bmatrix} a & \mathbf{f}^H \\ \mathbf{f} & \mathbf{Z} \end{bmatrix} \qquad \mathbf{C}(\ell+1)+\mathbf{R}=\begin{bmatrix} \mathbf{Z} & \mathbf{h} \\ \mathbf{h}^H & c \end{bmatrix} \tag{3.5}$$

where a and c are scalars, $\mathbf{f}$ and $\mathbf{h}$ are $(N-1)\times 1$ vectors, $\mathbf{Z}$ is a $(N-1)\times(N-1)$ matrix, and, assuming white noise, $\mathbf{R}=\sigma_v^2\mathbf{I}$. This structure allows the matrix inversion lemma to be utilized after applying a permutation resulting in

$$\left(\mathbf{C}(\ell+1)+\mathbf{R}\right)^{-1}=\mathbf{F}^{-1}-\mathbf{F}^{-1}\mathbf{U}\left(\mathbf{\Gamma}^{-1}+\mathbf{V}^H\mathbf{F}^{-1}\mathbf{U}\right)^{-1}\mathbf{V}^H\mathbf{F}^{-1} \tag{3.6}$$

where $\mathbf{F}=\begin{bmatrix} \mathbf{Z} & \mathbf{f} \\ \mathbf{f}^H & a \end{bmatrix}$, $\mathbf{U}=\begin{bmatrix} \left(\tilde{\mathbf{h}}-\tilde{\mathbf{f}}\right) & \mathbf{e}_N & \mathbf{e}_N \end{bmatrix}$, $\mathbf{V}=\begin{bmatrix} \mathbf{e}_N & \left(\tilde{\mathbf{h}}-\tilde{\mathbf{f}}\right) & \mathbf{e}_N \end{bmatrix}$, and $\mathbf{\Gamma}=diag\{1 \quad 1 \quad (c-a)\}$, in which $\tilde{\mathbf{h}}=\begin{bmatrix}\mathbf{h}^T & 0\end{bmatrix}^T$, $\tilde{\mathbf{f}}=\begin{bmatrix}\mathbf{f}^T & 0\end{bmatrix}^T$, and the $N\times 1$ elementary vector $\mathbf{e}_N=\begin{bmatrix}0 & \cdots & 0 & 1\end{bmatrix}^T$. Note $\mathbf{F}^{-1}$ can easily be obtained by applying a permutation matrix to the inverse at the current range cell $\left(\mathbf{C}(\ell)+\mathbf{R}\right)^{-1}$. Thus, the inverse correlation matrix at the current range cell can be efficiently computed when the previous correlation matrix inverse is available. However, at the initial range cell the standard inverse must be computed with a computational cost on the order of N^3 complex multiplies. Hence, as stated in [12], if the range profile is long enough ($L >> N$), such that the computation of

the initial inverse does not overwhelm the computational cost of the remaining range cells, the complexity of the algorithm can be reduced by an order of magnitude from $O(N^3)$ to $O(N^2)$ per range cell. This fast update technique will be referred to when discussing the implementation and computational complexity of Fast APC.

3.3.1 Efficient Implementation of Fast APC

For the two embodiments of the Fast APC algorithm the adaptive filters for each successive range cell only necessitate the update of a single $K \times K$ matrix with the other $M-1$ matrices having already been determined at a previous range delay. The remaining reduced-dimension signal correlation matrix can be computed efficiently via the fast matrix update discussed in the previous section. However, the particular structure of the update for Fast APC is dependent on the segmenting scheme. The following details the particular implementation for the decimation and contiguous embodiments of Fast APC.

Decimation FAPC can be implemented such that $M-1$ of the reduced-dimension signal correlation matrices needed to compute the unique pulse compression filter at each range can be replaced by matrices available from the determination of the previous range cell estimate. Also, the M^{th} matrix $\widetilde{\mathbf{C}}_{D,M-1}(\ell+1)$ can be obtained by applying the fast matrix update to $\widetilde{\mathbf{C}}_{D,0}(\ell)$. Consider the matrices for the estimation of the ℓ^{th} range cell from (2.25), given as

$$\widetilde{\mathbf{C}}_{D,m}(\ell)=\sum_{i=0}^{M-1}\sum_{k=-K+1}^{K-1}\rho(\ell+Mk-i+m)\,\widetilde{\mathbf{d}}_{i,k}\,\widetilde{\mathbf{d}}_{i,k}^{H} \tag{3.7}$$

and the $(\ell+1)^{\text{th}}$ range cell, denoted as

$$\widetilde{\mathbf{C}}_{D,m}(\ell+1)=\sum_{i=0}^{M-1}\sum_{k=-K+1}^{K-1}\rho(\ell+1+Mk-i+m)\,\widetilde{\mathbf{d}}_{i,k}\,\widetilde{\mathbf{d}}_{i,k}^{H} \tag{3.8}$$

for $m=0,1,\cdots,M-1$. Upon direct inspection of (3.7) and (3.8), it is evident that

$$\widetilde{\mathbf{C}}_{D,m}(\ell+1)=\widetilde{\mathbf{C}}_{D,m+1}(\ell) \tag{3.9}$$

for $m=0,1,\cdots,M-2$ thus, $M-1$ of the signal correlation matrix inverses do not need to be computed for any range cell after the initial cell.

Referring to Fig. 2.2, where $N=4$ and $M=2$, recall that the elements within ovals and squares represent the terms of the full-dimension matrix $\mathbf{C}(\ell)$ that constitute $\widetilde{\mathbf{C}}_{D,0}(\ell)$ and $\widetilde{\mathbf{C}}_{D,1}(\ell)$, respectively. Also, note that relative to the full-dimension matrix $\mathbf{C}(\ell+1)$, the elements within squares also represent $\widetilde{\mathbf{C}}_{D,0}(\ell+1)$ and thus the inverse of this matrix need not to be recomputed. The terms within octagons represent $\widetilde{\mathbf{C}}_{D,1}(\ell+1)$, which upon referring to (3.5), is related to $\widetilde{\mathbf{C}}_{D,0}(\ell)$ in a similar manner as the full-dimension signal correlation matrices $\mathbf{C}(\ell+1)$ and $\mathbf{C}(\ell)$. Thus, $\widetilde{\mathbf{C}}_{D,1}(\ell+1)$ can be obtained via a fast matrix update applied to the permutation of $\widetilde{\mathbf{C}}_{D,0}(\ell)$. Figure 3.3 is a block diagram illustrating how the *M* reduced-dimension signal correlation matrix inverses for the next successive range cell are obtained from the *M* reduced-dimension signal

correlation matrices at the current range cell. The last $M-1$ matrices at the current range cell are immediately reused as the first $M-1$ correlation matrix inverses at the next cell. The final inverse used to compute the M^{th} decimated filter segment at the new cell is found by applying the fast matrix update in to the first reduced-dimension inverse from the last cell, denoted $\widetilde{\mathbf{C}}_0^{-1}(\ell)$ in Fig. 3.3.

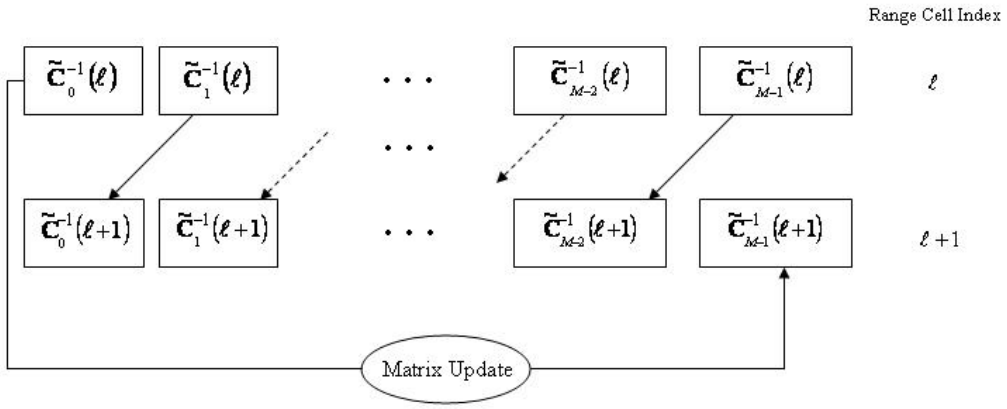

Figure 3.3 Reduced-Dimension Signal Correlation Matrix Update for Successive Range Cell Indices (Decimation FAPC)

For the contiguous FAPC implementation $M-1$ of the inverses required at the ℓ^{th} range cell can be stored in memory and re-used at the $(\ell+K)^{\text{th}}$ range cell. Thus, only a single reduced-dimension update is required to obtain the pulse compression filter for any range delay after the $(K-1)^{\text{th}}$. Examine the signal correlation matrices from (2.31) at the ℓ^{th} range cell

$$\widetilde{\mathbf{C}}_{C,m}(\ell) = \sum_{k=-N+1}^{K-1} \rho(\ell+k+Km)\,\widetilde{\mathbf{b}}_k \widetilde{\mathbf{b}}_k^H \tag{3.10}$$

and at the $(\ell+K)^{\text{th}}$ range cell

$$\widetilde{\mathbf{C}}_{C,m}(\ell) = \sum_{k=-N+1}^{K-1} \rho(\ell + K + k + Km)\, \widetilde{\mathbf{b}}_k \widetilde{\mathbf{b}}_k^H \tag{3.11}$$

for $m = 0,1,\cdots,M-1$. Upon inspection it is observed that

$$\widetilde{\mathbf{C}}_{C,m}(\ell + K) = \widetilde{\mathbf{C}}_{C,m+1}(\ell) \tag{3.12}$$

for $m = 0,1,\cdots,M-2$. Therefore at the $(\ell + K)^{\text{th}}$ range cell, $M-1$ of the inverse signal correlation matrices which were employed for the estimation of the ℓ^{th} range cell can be recalled from memory without re-computing. The remaining matrix can be computed using the fast matrix update.

Recall Figure 2.4, which depicts the full-dimension signal correlation matrices at the ℓ^{th} and $(\ell+1)^{\text{th}}$ range cells, and the outlined sub-matrices (boxes and octagons) represent the reduced dimension signal correlation matrices. For this example, $K = 2$ and thus the sub-matrix $\widetilde{\mathbf{C}}_{C,1}(\ell)$ two range cells later, will also be $\widetilde{\mathbf{C}}_{D,0}(\ell+2)$. Furthermore, the remaining matrix $\widetilde{\mathbf{C}}_{D,1}(\ell+2)$ has a structure such that it can be efficiently computed by a rank-3 update of $\widetilde{\mathbf{C}}_{D,1}(\ell+1)$. Generally speaking, Figure 3.4 depicts a block diagram of the progression of the stored matrices as the filter is computed for each range cell. It is illustrated in Fig. 3.4, that $((M-1)(K-1))$ of the previously used inverses must be stored in memory so that they can be re-used at a later range cell. In Fig. 3.4 each new inverse is introduced as a fast-update of the reduced-dimension correlation matrix used to determine the M^{th} filter segment at the previous range cell. After, being used the new inverse progresses through memory as indicated

until finally it is discarded after having been used to compute each of the M filter segments once (at different range cells).

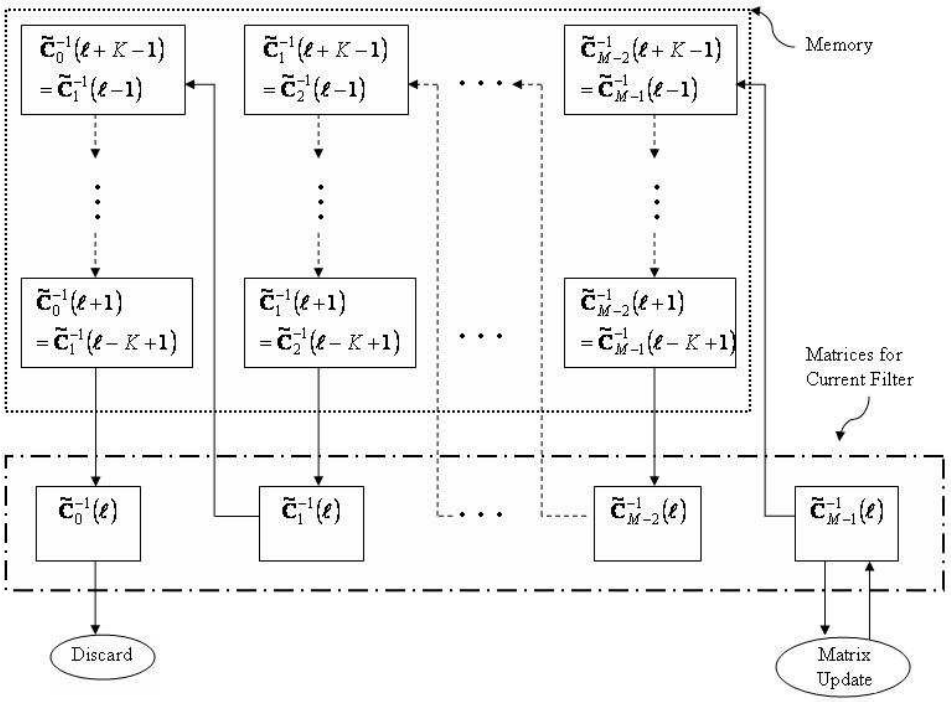

Figure 3.4 Reduced-Dimension Signal Correlation Matrix Update for Successive Range Cell Indices (Contiguous FAPC)

3.3.2 Computational Cost of Fast APC

Computational cost will be couched in terms of the approximate number of complex multiplies necessary to obtain the unique Fast APC filter at a single range cell. The computationally efficient matched filter requires N complex multiplies to determine the estimate for each range cell. First, the computational cost of full-dimension APC will be determined. Secondly, the computational complexity of Fast APC will be obtained and compared to the matched filter and APC.

Re-examine the full-dimension matrix update equation from (3.6)

$$\left(\mathbf{C}(\ell+1)+\mathbf{R}\right)^{-1} = \mathbf{F}^{-1} - \mathbf{F}^{-1}\mathbf{U}\left(\mathbf{\Gamma}^{-1} + \mathbf{V}^{H}\mathbf{F}^{-1}\mathbf{U}\right)^{-1}\mathbf{V}^{H}\mathbf{F}^{-1} \tag{3.13}$$

where $\mathbf{F}^{-1}$ is $N \times N$, $\mathbf{\Gamma}$ is 3×3, $\mathbf{U} = \left[\left(\tilde{\mathbf{h}} - \tilde{\mathbf{f}}\right) \quad \mathbf{e}_N \quad \mathbf{e}_N\right]$ and $\mathbf{V} = \left[\mathbf{e}_N \quad \left(\tilde{\mathbf{h}} - \tilde{\mathbf{f}}\right) \quad \mathbf{e}_N\right]$ are $N \times 3$ (recall $\mathbf{e}_N = \left[0 \quad \cdots \quad 0 \quad 1\right]^T$). $\mathbf{F}^{-1}$ is already known and the computation of $\mathbf{\Gamma}^{-1}$ is negligible. It can be shown that finding $\tilde{\mathbf{h}}$ and $\tilde{\mathbf{f}}$ requires $N(N-1)$ complex multiplies. The matrix $\mathbf{F}^{-1}\mathbf{U}$ requires only N^2 complex multiplies to determine because the product of the elementary vector $\mathbf{e}_N$ with a matrix does not require any additional operations. The product $\mathbf{V}^{H}\mathbf{F}^{-1}$ can be found directly from $\mathbf{F}^{-1}\mathbf{U}$ and thus requires no additional operations. However, determining the product $\mathbf{V}^{H}\mathbf{F}^{-1}\mathbf{U}$ requires $3N$ multiplies. The 3×3 inverse $\left(\mathbf{\Gamma}^{-1} + \mathbf{V}^{H}\mathbf{F}^{-1}\mathbf{U}\right)^{-1}$ requires approximately 27 multiplies and is therefore considered negligible. The only remaining product required to compute $\left(\mathbf{C}(\ell+1)+\mathbf{R}\right)^{-1}$ from (3.13) is

$$\left[\mathbf{F}^{-1}\mathbf{U}\right]_{N\times 3} \times \left[\left(\mathbf{\Gamma}^{-1} + \mathbf{V}^{H}\mathbf{F}^{-1}\mathbf{U}\right)^{-1}\right]_{3\times 3} \times \left[\mathbf{V}^{H}\mathbf{F}^{-1}\right]_{3\times N} \tag{3.14}$$

which requires $3N^2 + 9N$ complex multiplies. Thus determining the signal correlation matrix inverse incurs a computational cost of approximately $4N^2 + 12N$ multiplies at each range cell (not including computation of $\tilde{\mathbf{h}}$ and $\tilde{\mathbf{f}}$).

After obtaining the signal correlation matrix inverse the filter weights are obtained from

$$\mathbf{w}(\ell) = \rho(\ell)\left(\mathbf{C}(\ell) + \mathbf{R}\right)^{-1}\mathbf{s} \tag{3.15}$$

which necessitates $N^2 + N$ complex multiplies. The filter must then be applied to the length-N received signal vector $\mathbf{y}(\ell)$ which requires N complex multiplies. Computing and applying the APC filter yields a cost of $N^2 + 2N$ multiplies. Thus the total cost of the APC algorithm is $6N^2 + 13N$ complex multiplies per range cell at each adaptive stage.

The Fast APC algorithm requires updating only a single $K \times K$ reduced-dimension correlation matrix inverse at each range cell. The computation required to determine the $K \times K$ matrix $\left(\widetilde{\mathbf{C}}_m(\ell+1) + \widetilde{\mathbf{R}}_m\right)^{-1}$ is analogous to that required by the full-dimension version $\left(\mathbf{C}(\ell+1) + \mathbf{R}\right)^{-1}$ with $N = K = \frac{N}{M}$ yielding a cost of $4\frac{N^2}{M^2} + 12\frac{N}{M}$ multiplies. However, it can be shown that only a portion of the vectors $\widetilde{\mathbf{f}}$ and $\widetilde{\mathbf{h}}$ (from the full-dimension case) need to be determined reducing their computation to $2\frac{N^2}{M} - \frac{N^2}{M^2} - 2N + \frac{N}{M}$ multiplies. The filter weights are then determined as

$$\widetilde{\mathbf{w}}_m(\ell) = \frac{\rho(\ell)}{M}\left(\widetilde{\mathbf{C}}_m(\ell) + \widetilde{\mathbf{R}}_m\right)^{-1}\widetilde{\boldsymbol{\xi}}_m \tag{3.16}$$

for $m = 0,1,\cdots,M-1$, where $\widetilde{\boldsymbol{\zeta}}_m$ represents $\widetilde{\mathbf{d}}_{m,0}$ or $\widetilde{\mathbf{b}}_{\beta(m)}$ for decimation or contiguous FAPC, respectively. The computation required to obtain all of the segments given in (3.16) is $M\left(\frac{N^2}{M^2}+\frac{N}{M}\right)$ complex multiplies. The filter is finally applied requiring N complex multiplies. The total resulting cost of Fast APC is $N^2\left(\frac{3}{M^2}+\frac{3}{M}\right)+\frac{13N}{M}$ multiplies per range cell per adaptive stage.

Parallel processing can be used to further reduce the computational cost of the Fast APC algorithm. The needed portions of $\widetilde{\mathbf{f}}$ and $\widetilde{\mathbf{h}}$ can be determined utilizing parallel multiplication reducing their computational cost to $2N$ multiplies. The M filter segments from (3.16) can also be computed in parallel incurring a reduced cost of $\left(\frac{N^2}{M^2}+\frac{N}{M}\right)$ multiplies. Thus, parallelized Fast APC yields a total computational cost of $\frac{5N^2}{M^2}+N\left(3+\frac{13}{M}\right)$ at each range cell per adaptive stage.

The computational cost (per range cell) of the matched filter, APC, and parallelized Fast APC vs. the length of the transmit waveform, *N*, is illustrated in Fig. 3.5 on a log *N* scale. The matched filter incurs a cost of *N* multiplies per range cell and is thus is a flat line in Fig 3.5. The APC and Fast APC curves include the matched filter followed by one adaptive stage. It is evident that as the segmenting factor is increased the computational cost of Fast APC is reduced but

as *M* is increased the performance of the algorithm degrades which will be shown in the next chapter.

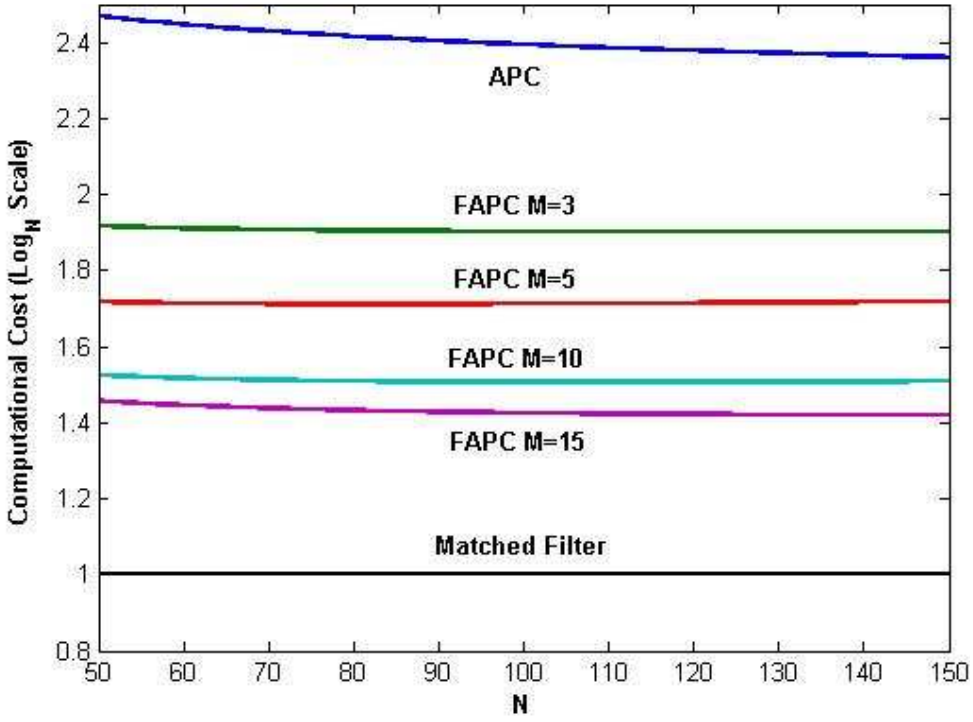

Figure 3.5 Computational Cost (per range cell) of Parallelized Fast APC

CHAPTER 4 SIMULATION RESULTS

Simulations were performed using a Lewis-Kretschmer P3 code [3] given as

$$s(n) = e^{j\frac{\pi}{N}n^2} \tag{4.1}$$

for $n = 0,1,\cdots N-1$, where N corresponds to the length of the transmitted waveform. Scatterers are represented as point targets in additive white Gaussian noise (AWGN) and stated SNR values are post pulse-compression.

Increased-dimensionality results will be presented for the over-sampled versions of APC and Least-Squares. The effects of straddling loss as well as continuous and realistic discrete time waveforms will be examined. The reduced-dimensionality results will then be presented for several scenarios. The new Fast APC algorithm will be compared to the computationally efficient matched filter and the APC algorithm which provides an exceptionally accurate estimate of the range profile.

4.1 Increased-Dimensionality Results

Results presented here will compare the performance of over-sampled APC and Least-Squares to each other and to the matched filter. First the modeling of over-sampled transmit waveforms will be discussed. Next,

straddling loss at nominal resolution will be examined. Third, the super-resolution capabilities of the over-sampled (by $\Lambda = 5$) versions of APC and Least-Squares will be explored for cases with and without diagonal loading. Finally, probability of separation results will be presented for the cases with super-resolution factors of $\Lambda = 2$ and $\Lambda = 3$.

4.1.1 Waveform Modeling

The over-sampled filter representations for APC and Least-Squares in (2.6) and (2.10), respectively, require over-sampling the transmitted waveform. For a continuous waveform, over-sampling is straightforward and is currently common for systems employing digital pulse compression. However, ideal discrete waveforms such as polyphase codes are constant over discrete phase values, often referred to as chip intervals, (which determines the range resolution) and possess a discontinuity between each chip. In reality, these waveforms are implemented with a finite transition between successive chips that determines the effective overall bandwidth of the waveform. As an example, a close-up comparison of a segment of a sampled linear frequency modulation (LFM) waveform and both an ideal and realistic discrete waveform is depicted in Fig. 4.1. While the continuous waveform exhibits smooth phase transitions, the ideal discrete waveform, and to a lesser degree the realistic discrete waveform, demonstrate much sharper phase transitions. It is these sharp transitions that determine the actual bandwidth of the discrete waveform.

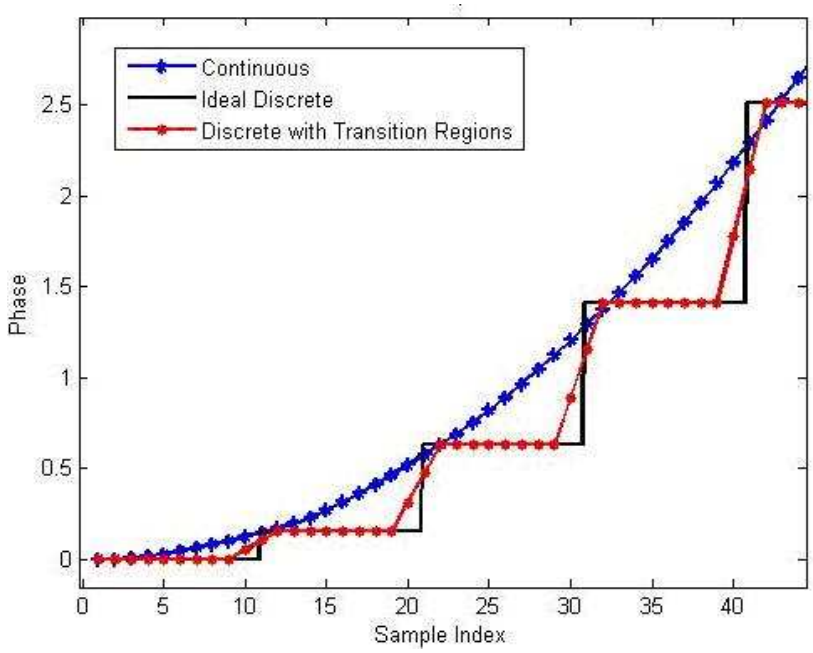

Figure 4.1 Close-Up of Over-Sampled Waveform Models

Since the bandwidth directly determines the range resolution for continuous waveforms, discrete waveforms therefore require greater bandwidth to achieve the same nominal resolution (dependent on the chip width for discrete waveforms). However, due to the presence of the extraneous bandwidth corresponding to the transition regions, discrete waveforms can be expected to provide better super-resolution performance than their continuous counterparts. In order to maintain a fair comparison in terms of resolution, the continuous and discrete waveforms employed in the increased-dimensionality results will possess the same nominal range resolution as provided by the matched filter.

Both the continuous and discrete waveforms are derived from the same original waveform, a length $N = 20$ P3 code which is known to be a sampled version of an LFM waveform. The continuous waveform is modeled by over-sampling the P3 function in (4.1) by 10 and interpolating such that the resultant waveform is as shown in Fig. 4.1 with smooth phase transitions. In contrast the discrete waveform utilizes the N discrete phases of the P3 code repeated 10 times to produce the ideal discrete over-sampled waveform. Then, the samples constituting the final sample of a given chip and the first sample of the following chip are phase interpolated as depicted in Fig. 4.1 to generate the transition regions between successive chips thus producing the realistic discrete over-sampled waveform. Note that by phase interpolating the constant modulus nature of the waveform is preserved.

4.1.2 Straddling Loss

Straddling loss occurs when the received signal is sampled such that a reflected version of the transmitted waveform coinciding with a target aligns with the transition regions of the over-sampled discrete waveform. To first establish a benchmark for performance at nominal resolution, the realistic discrete over-sampled waveform is convolved with a range profile containing two targets. The received signal is down-sampled by 10 such that processing will be performed at the nominal resolution. In Figure 4.2, the scatterer at range index 575 occurs in sync with the flat portion of the chip while the scatterer at range index 510 aligns

with the transition region and thus will result in a straddling loss. Figure 4.2 illustrates the range profile estimates for the normalized matched filter, Least-Squares, and the APC algorithm each using the nominal P3 code and compared to the true range profile. It is observed from Fig. 4.2 that both APC and Least-Squares exhibit lower range sidelobes than the matched filter, with APC slightly outperforming Least-Squares.

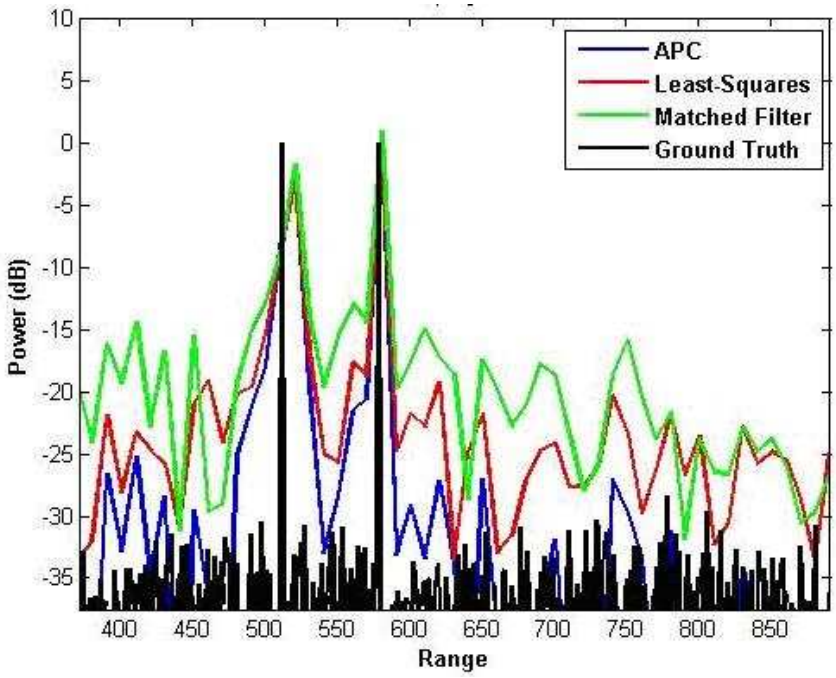

Figure 4.2 Straddling Loss at Nominal Resolution

4.1.3 Un-Loaded Super-Resolution

The APC and Least-Squares algorithms are capable of achieving range super-resolution for both continuous and discrete waveforms when they are appropriately over-sampled. As mentioned earlier, the waveforms are over-sampled by a factor of 10 when convolved with the true range profile followed by down-sampling by 2 to model the received signal with the possibility for straddling losses between samples. The resulting received signal and waveform used for processing are over-sampled by $\Lambda = 5$. Figures 4.3 and 4.4 display the results for the over-sampled continuous and realistic discrete over-sampled waveforms, respectively, when employing the unloaded versions of Least-Squares from (3) and APC from (5). The true range profile consists of two scatterers at range indices 543 and 549 that are in sync with the receive sampling (*i.e.* no straddling losses) and two scatterers at range indices 485 and 491 that are delay shifted thus resulting in straddling losses. Note that each pair of scatterers, which are spaced by two super-resolved range cells, reside in the same nominal range cell and thus cannot be resolved by the matched filter.

For the over-sampled continuous waveform, the results are shown in Fig. 4.3 where it is observed that, in terms of depicting the locations of the scatterers and otherwise suppressing sidelobes, poor performance is obtained for the unloaded Least-Squares while better performance is achieved for the unloaded APC algorithm. APC is able to resolve both pairs of scatterers yet Least-Squares is only able to resolve the second pair. Furthermore, due to ill-conditioning

Least-Squares exhibits rather high sidelobe levels, in some places even higher than the matched filter.

For the realistic discrete over-sampled waveform, Fig. 4.4 illustrates the super-resolution performance for APC and Least-Squares. First, note that the matched filter performance for both the continuous and discrete waveforms is virtually identical as these two waveforms provide the same nominal resolution. However, unlike for the over-sampled continuous waveform, both APC and Least-Squares now resolve both sets of scatterers with the sidelobe levels for Least-Squares undergoing the most noticeable reduction relative to Fig. 4.3 (though the effects of ill-conditioning can still be observed). This improvement is not surprising because as discussed earlier the realistic discrete waveform possesses a higher bandwidth than its continuous counterpart thus enabling greater range diversity when super-resolution methods are employed. In addition, the effects of straddling have been reduced as seen in Fig. 4.4 when compared to the nominal resolution case in Fig. 4.2. This improvement can be attributed to the over-sampled realistic discrete waveform used for processing providing a more accurate representation of the transmit waveform.

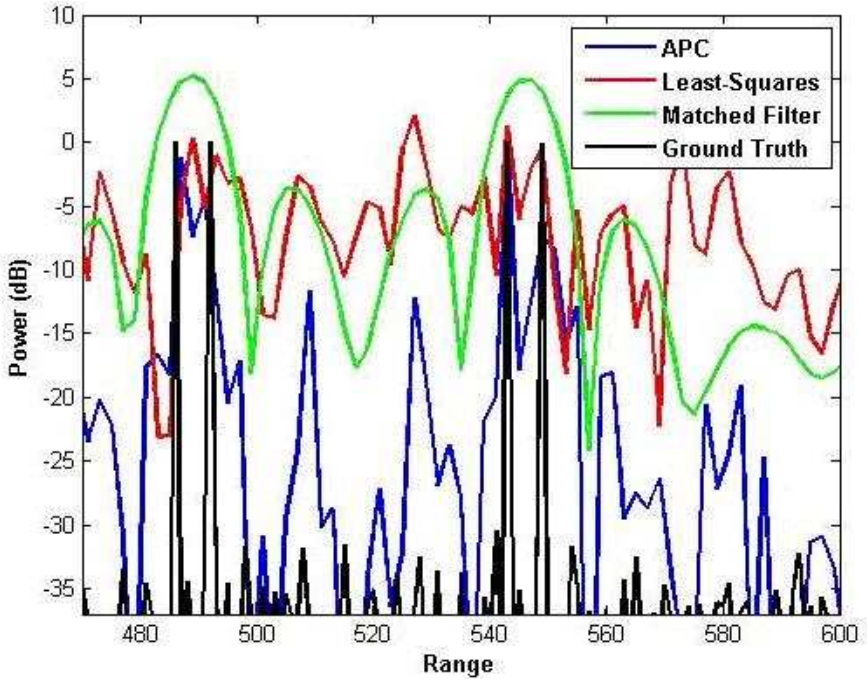

Figure 4.3 Super-Resolution, Continuous Waveform, No Diagonal Loading

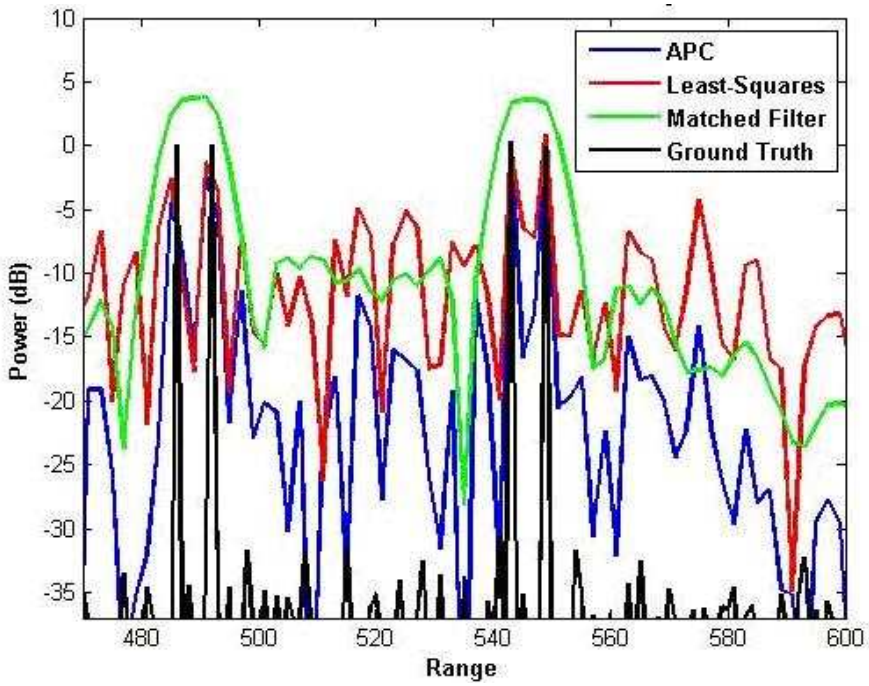

Figure 4.4 Super-Resolution, Realistic Discrete Waveform, No Diagonal Loading

4.1.4 Loaded Super-Resolution

The super-resolution estimates for the APC and Least-Squares algorithms can be improved by employing the diagonally loaded versions in (3.2) and (3.3), respectively, to reduce the noise enhancement effects of moderate matrix ill-conditioning. This improvement is illustrated in Figs. 4.5 and 4.6 for the same range profile as considered previously using the over-sampled continuous waveform and the realistic discrete over-sampled waveform, respectively.

For the over-sampled continuous waveform, the loading factors for Least-Squares and APC were set as $\delta = 0.5$ and $\gamma = 5$, respectively. These values were found to work well and no claim is made to their optimality. The results for this case are shown in Fig. 4.5 where considerable improvement is observed relative to the unloaded case of Fig. 4.3. Now the loaded versions of Least-Squares and APC resolve both pairs of scatterers with the sidelobe levels for loaded APC found to be dramatically lower than loaded Least-Squares and the unloaded version of APC.

When the realistic discrete over-sampled waveform is employed, the loading factors for Least-Squares and APC were set as $\delta = 2$ and $\gamma = 20$, respectively. As with the continuous case, these values were found to work well and are not necessarily optimal. Figure 5.6 depicts the results for this case in which it is found that loaded Least-Squares shows a marked improvement over when the continuous waveform was employed. Loaded APC yields more modest improvement for the discrete waveform relative to the continuous evidenced by

the deeper nulls between each pair of scatterers. Although, compared to the unloaded and loaded versions of Least-Squares and unloaded APC, the performance improvement for loaded APC is substantial.

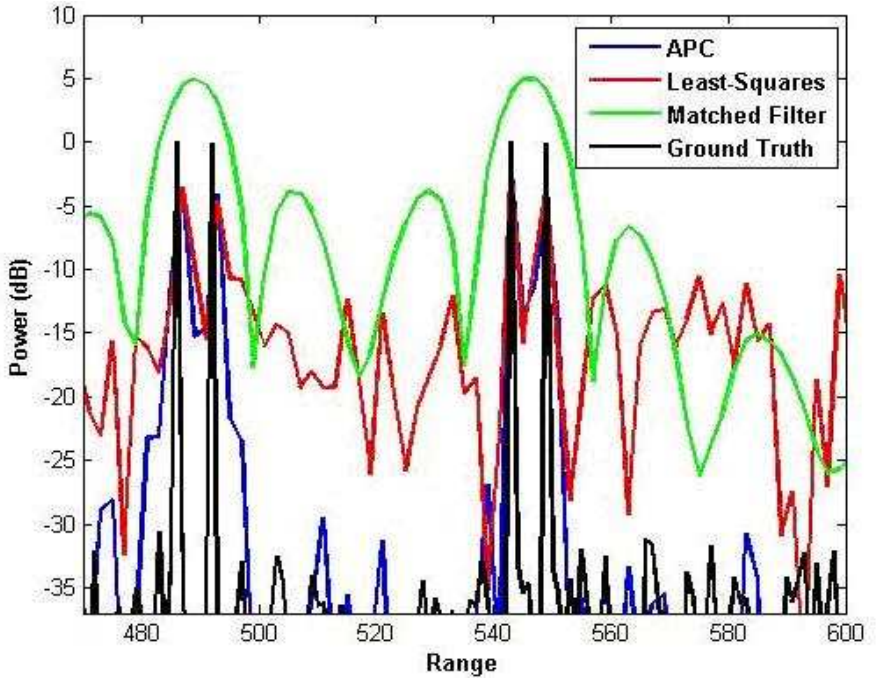

Figure 4.5 Super-Resolution, Continuous Waveform, with Diagonal Loading

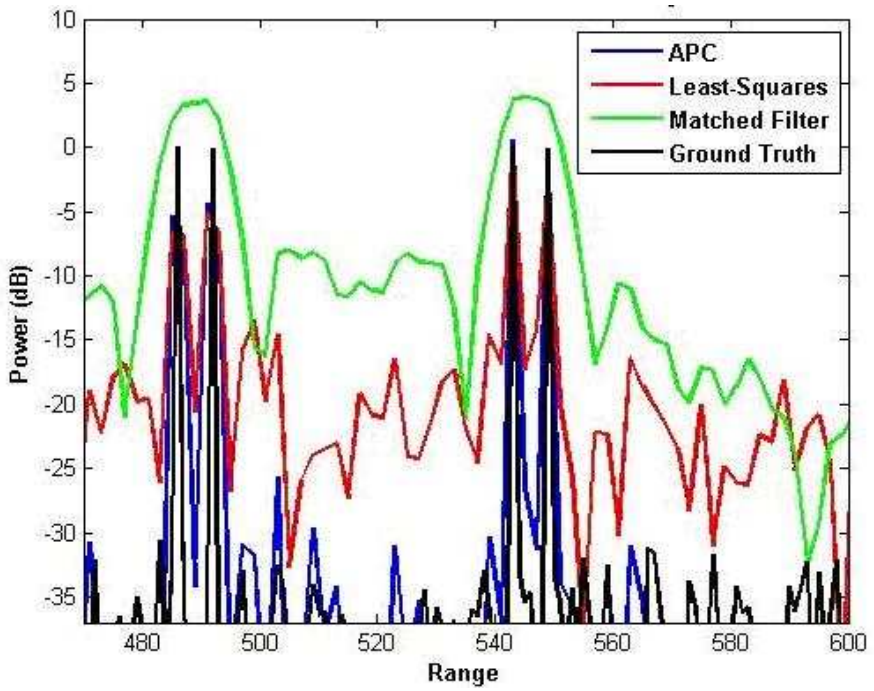

Figure 4.6 Super-Resolution, Realistic Discrete waveform, with Diagonal Loading

4.1.5 Probability of Separation

Probability of separation was determined for APC and Least-Squares (LS) when the received signal and transmit waveform were over-sampled by factors of $\Lambda = 2$ and $\Lambda = 3$. The simulation scenario contained two targets of equal SNR separated by a single range cell (at the over-sampled resolution). The transmitted waveform was a P3 code with a nominal length of $N = 60$ which was then over-sampled by 12, convolved with the range profile, and along with the received signal, down-sampled by 6 and 4 resulting in super-resolution factors of $\Lambda = 2$ and $\Lambda = 3$, respectively. The scatterers, which were in sync with the receive

sampling (*i.e.* no straddling loss), were said to be resolved if the power estimate in the empty range cell between them was at least 3 dB below the lower of the two power estimates in the surrounding range cells containing the targets. The SNR was varied and the results were averaged over 100 runs to determine the probability of resolution curves shown in Figs. 4.7 and 4.8 for over-sampling factors of $\Lambda = 2$ and $\Lambda = 3$, respectively. Note that detectability was not taken into consideration as the SNR of the scatterers was eventually reduced to 0 dB.

In Fig. 4.7 when the nominal resolution is enhanced by a factor of $\Lambda = 2$ the realistic discrete waveform provides a slight improvement over the continuous waveform for both algorithms. The performance of the continuous waveform degrades significantly when the resolution is enhanced by a factor of $\Lambda = 3$ as seen in Fig. 4.8. In both cases the over-sampled version of APC marginally outperforms the over-sampled Least-Squares approach. However, one might surmise that Adaptive Pulse Compression will provide a superior estimate in a dense channel given the sidelobe levels of the Least-Squares algorithm in Figs. 4.4 and 4.6.

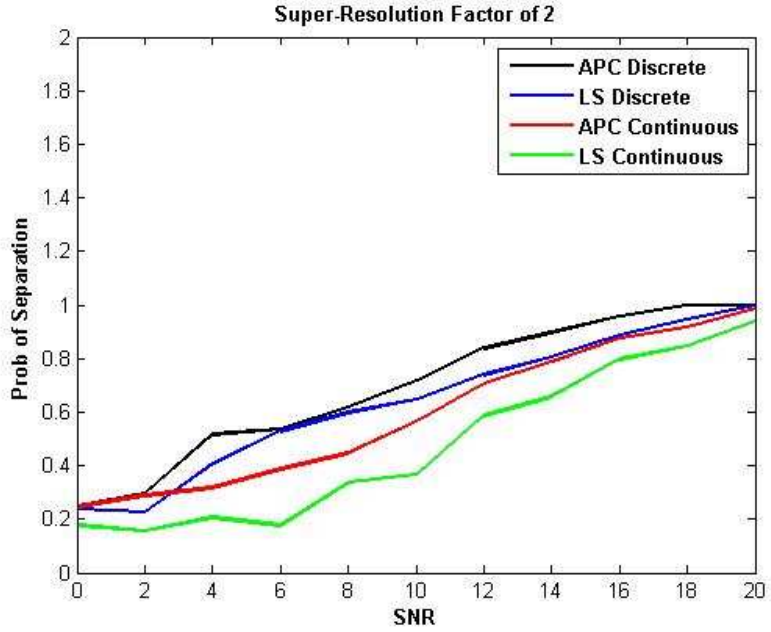

Figure 4.7 Probability of Separation, Super-Resolution by a Factor of $\Lambda = 2$

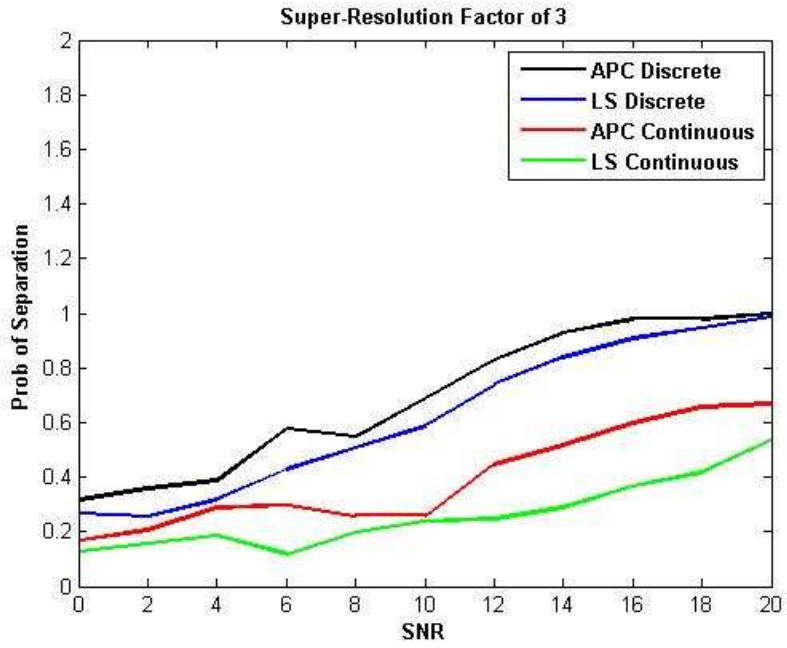

Figure 4.8 Probability of Separation, Super-Resolution by a Factor of $\Lambda = 3$

4.2 Reduced-Dimensionality Results

Simulation results will demonstrate the performance of the two embodiments of Fast APC compared to the original APC method and the normalized matched filter. The first scenario consists of a large scatterer within close proximity of a small scatterer where the range sidelobes of the match filter are known to mask the small target. Next, the Doppler mismatch characteristics of Fast APC will be examined in a similar scenario where the large scatterer is moving radially outward from the radar. The third and fourth simulations contain a randomly populated range profile and a random range profile with scatterer motion, respectively. Finally, probability of detection results for the masking scenario will be presented. The waveform used for all reduced-dimensionality results was a length $N = 60$ P3 code.

4.2.1 Masking Scenario

The first scenario consists of two point scatterers, one large (SNR of 60 dB) and one small (SNR of 20 dB). The scatterers are separated by three range cells. The normalized matched filter provides the initial range profile estimate for both embodiments of Fast APC as well as APC, each of which performs two adaptive stages. Figures 4.9 and 4.10 show the results of the decimation and contiguous FAPC algorithms, respectively. Here the number of blocks used is $M = 4$ with a block size of $K = 15$. Both embodiments of Fast APC achieve performance on the level of the original APC algorithm, suppressing the sidelobes

into the noise such that the small target is detectable, where as the matched filter's range sidelobes prevent detection of this scatterer as expected. As in [12] a heuristic floor has been placed on the power estimates to avoid ill-conditioning of the signal correlation matrices at the following stage. The flat-lining effect seen in Figs. 4.9 and 4.10 is a result of this floor, which has been placed 3 dB below the noise as Fast APC tends to suppress the interference below the noise floor. However, this increased suppression does not result in enhanced sensitivity and the analysis of this effect has been left as future work.

The performance of the Fast APC algorithm in the masking scenario degrades as M becomes large (or conversely K becomes small) this is shown in Figures 4.11 and 4.12 where the above scenario is duplicated for decimation and contiguous FAPC, respectively, with $M = 10$ ($K = 6$). Decimation FAPC suffers a 5 dB loss for the small scatterer and contiguous FAPC now actually suppresses the small scatterer. This effect has been regularly observed and is more pronounced as M increases or as the power of the masked scatterer approaches the noise floor. It is believed to be an effect of the reduced-dimension approximation as the full-dimension APC yields no such effects. Mean Squared Error (MSE) results for this scenario can be found in Table I.

Table I MSE Results in dB**,** Masking Scenario

	M = 4	**M = 10**
Matched Filter	**-33**	**-33**
APC	**-60**	**-60**
Decimation FAPC	**-60**	**-58**
Contiguous FAPC	**-59**	**-56**

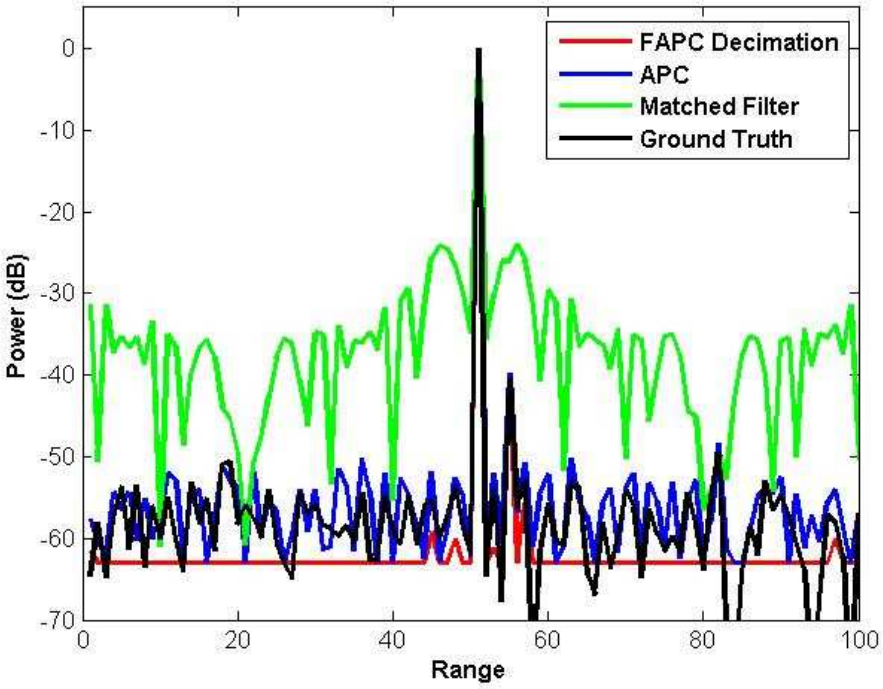

Figure 4.9 Masking Scenario, Decimation FAPC, *M = 4*

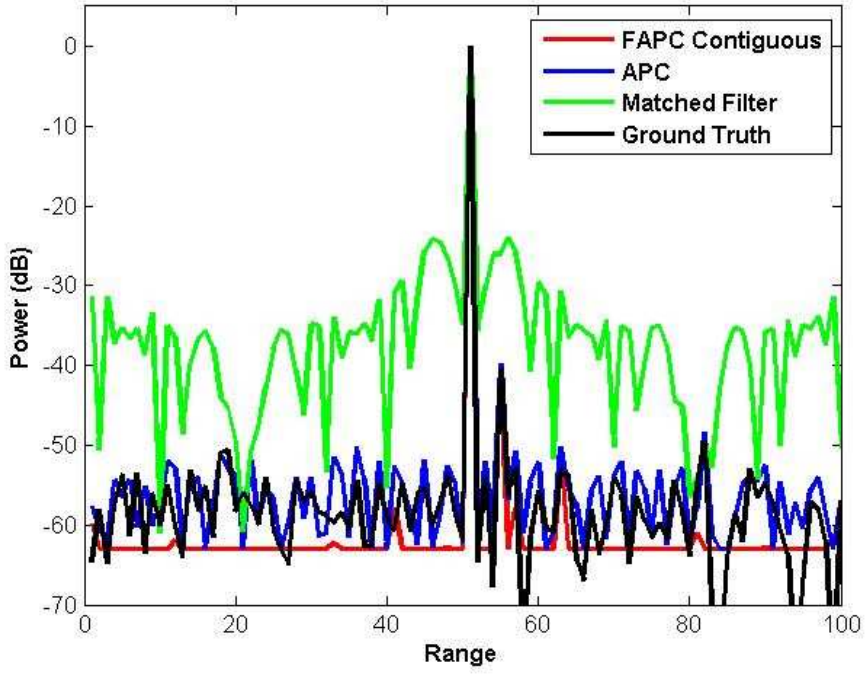

Figure 4.10 Masking Scenario, Contiguous FAPC, *M = 4*

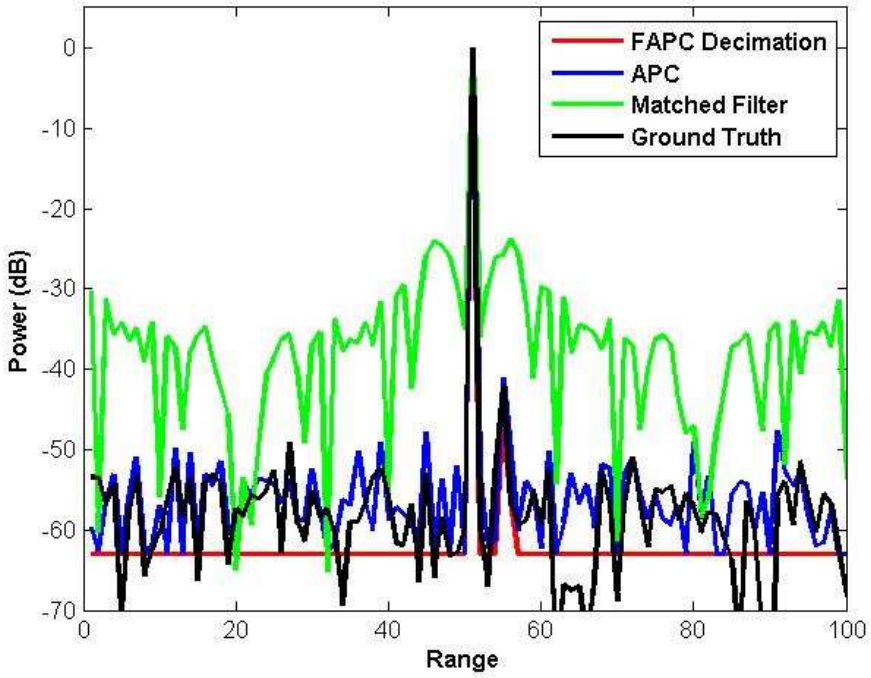

Figure 4.11 Masking Scenario, Decimation FAPC, *M = 10*

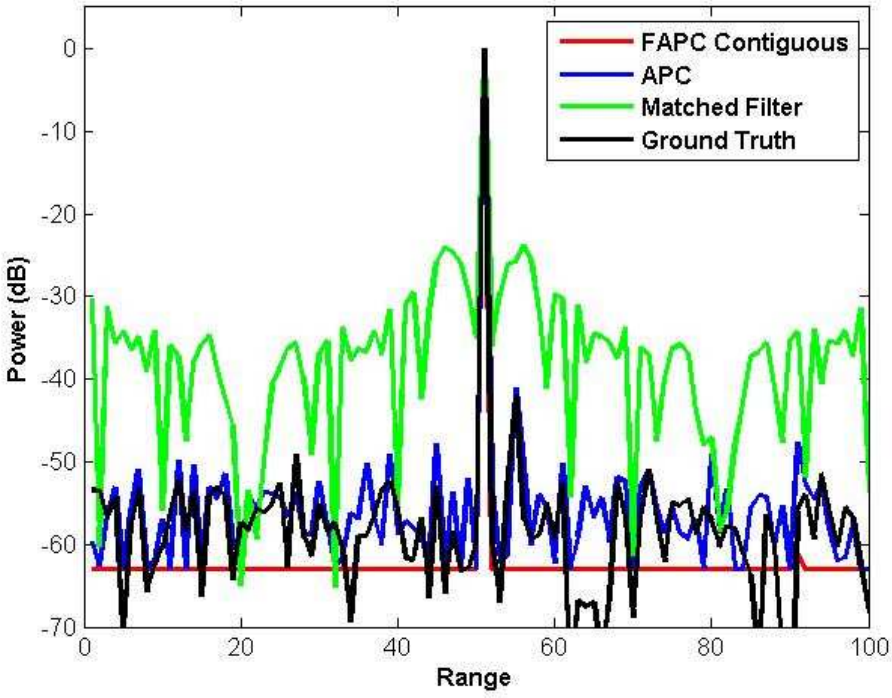

Figure 4.12 Masking Scenario, Contiguous FAPC, *M = 10*

4.2.2 Masking Scenario with Doppler

For the second case the large scatterer is traveling radially away from the radar such that a Doppler shift is induced analogous to a Mach 2 scatterer illuminated by a 1 μs pulse at S-band. Figs. 4.13 and 4.14 depict the results when 3 adaptive stages are performed for $M = 4$ and $K = 15$. As before, the matched filter's range sidlobes prevent detection of the smaller scatterer, but now the APC and decimation FAPC algorithms exhibit some range sidelobes caused by Doppler mismatch greatly decreasing the detectability of the small target. However, contiguous FAPC is found to be more tolerant to Doppler mismatch and thus the small scatterer remains easily detectable, as seen in Figure 4.14.

The improved robustness to Doppler mismatch by contiguous FAPC is due to the smaller overall Doppler shift over the reduced-dimension filter (K range cells instead of $K = NM$ for APC) thus resulting in less mismatch. Alternatively, one could view this as the contiguous FAPC placing wider nulls in Doppler as a result of its shorter temporal extent relative to either APC or decimation FAPC. Fig 4.15 displays a cut from an ambiguity diagram showing the interference cancelling nulls of APC and the two embodiments of Fast APC versus Doppler shift. The scenario used to produce Fig. 4.15 is similar to that depicted in Figs. 4.13 and 4.14 and contained a large moving target three range cells away from a small scatterer. The MSE results for this case are displayed in Table II.

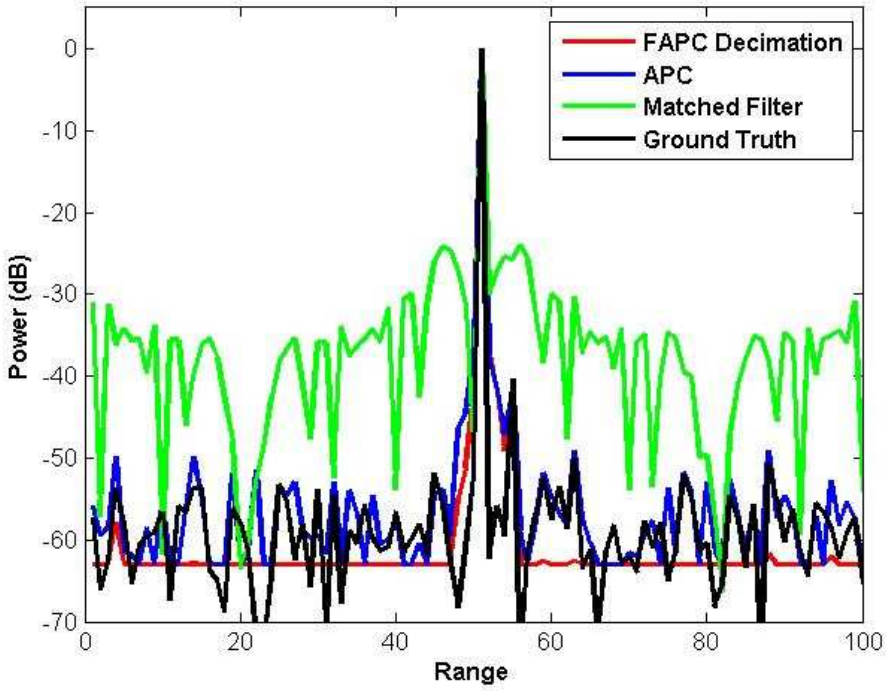

Figure 4.13 Masking Scenario with Doppler, Decimation FAPC, *M = 4*

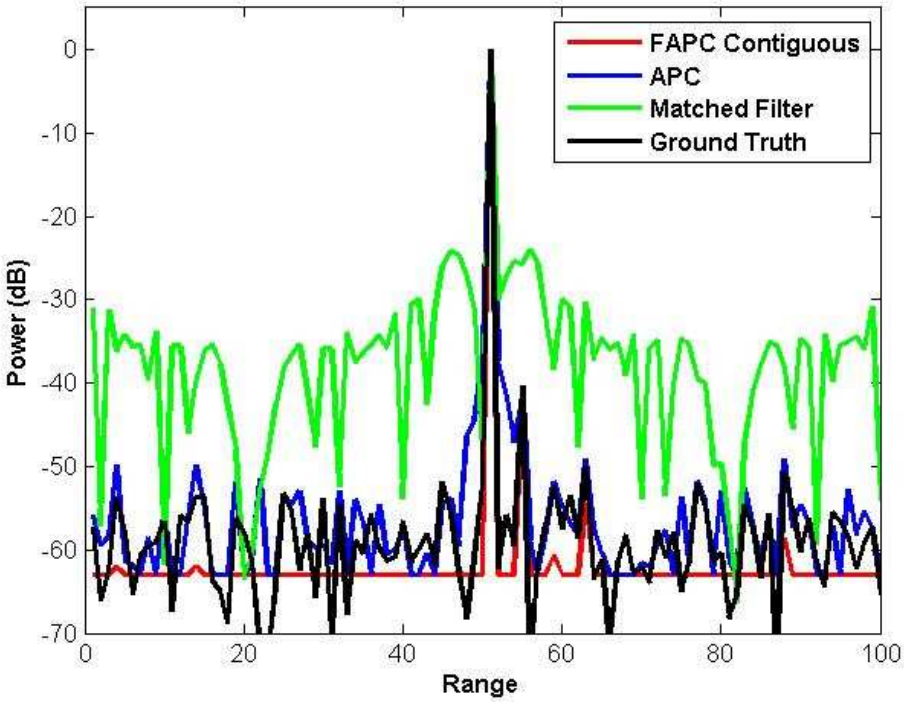

Figure 4.14 Masking Scenario with Doppler, Contiguous FAPC, *M = 4*

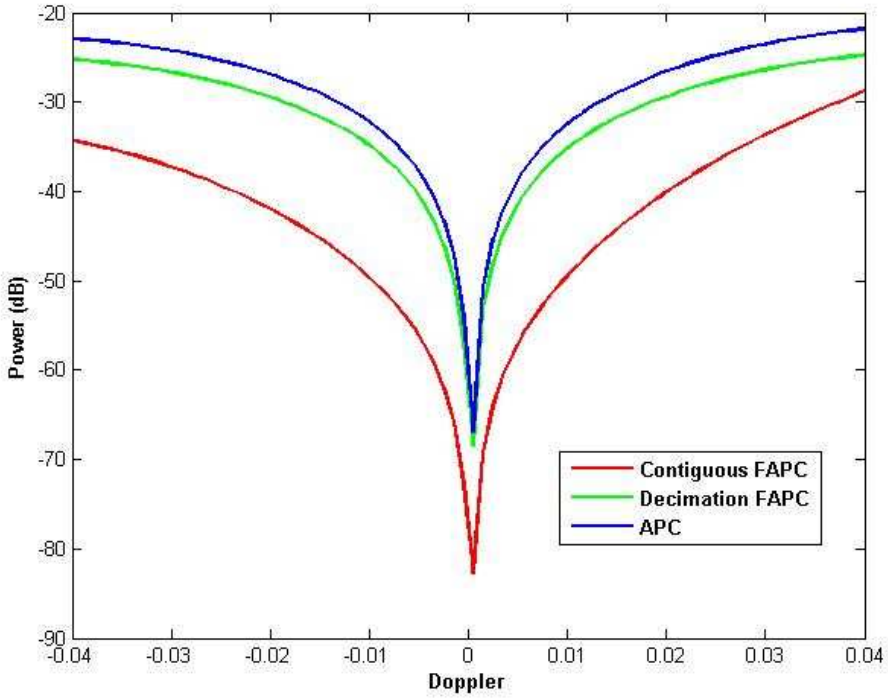

Figure 4.15 Doppler Cross-Section of Ambiguity Diagram for Range Offset Containing Interference Null

Table II MSE Results in dB**,** Masking Scenario with Doppler

	M = 4
Matched Filter	**-33**
APC	**-46**
Decimation FAPC	**-46**
Contiguous FAPC	**-47**

4.2.3 Dense Scenario

A range profile with several randomly distributed scatterers with varying powers will now be considered. Figure 4.16 displays the results for decimation FAPC when 3 adaptive stages are performed with $M = 4$. The decimation FAPC embodiment performs rather poorly suppressing some of the smaller scattereres

into the noise. Figure 4.17 shows the results for 3 adaptive stages of contiguous FAPC with $M = 4$. The performance of the contiguous FAPC embodiment is comparable to APC, unmasking several scatterers that reside below the matched filter's sidelobe level.

The performance of both algorithms degrade significantly, as expected, in a dense environment as block size decreases, which can be seen in Figures 4.18 and 4.19 for decimation and contiguous FAPC, respectively. It has been observed that contiguous FAPC generally outperforms the decimation embodiment in a dense environment. The resulting MSE for each algorithm is shown in Table III.

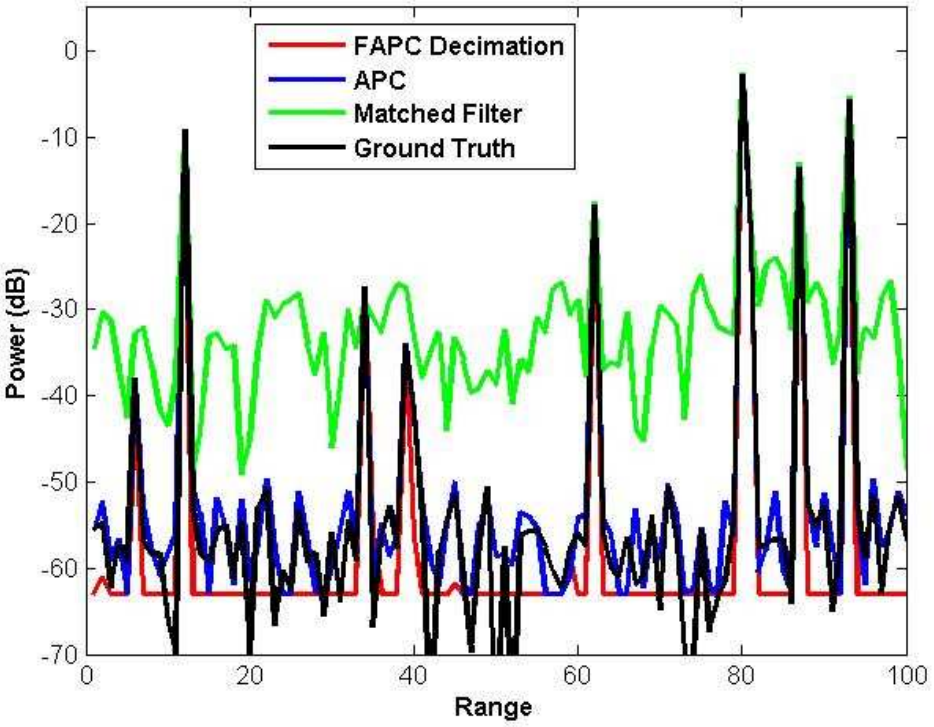

Figure 4.16 Dense Scenario, Decimation FAPC, *M = 4*

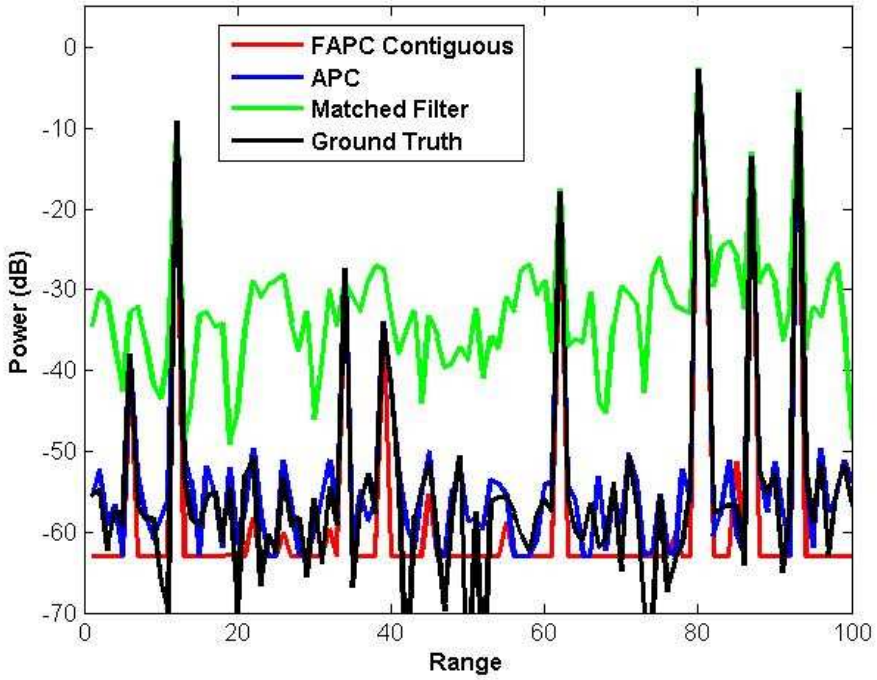

Figure 4.17 Dense Scenario, Contiguous FAPC, *M = 4*

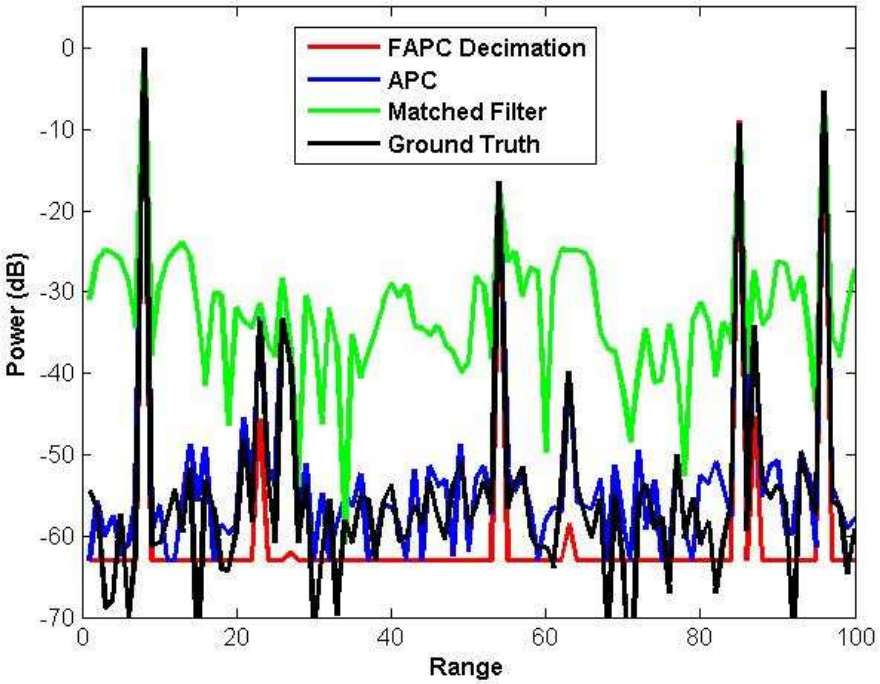

Figure 4.18 Dense Scenario, Decimation FAPC, *M = 10*

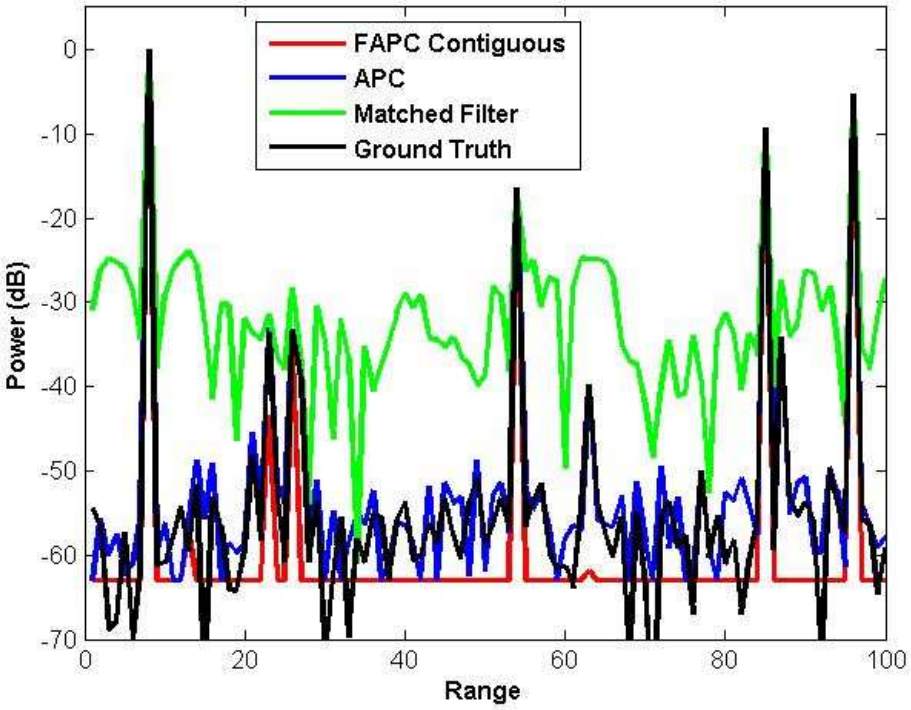

Figure 4.19 Dense Scenario, Contiguous FAPC, *M = 10*

Table III MSE Results in dB**,** Dense Scenario

	M = 4	**M = 10**
Matched Filter	**-32**	**-32**
APC	**-61**	**-58**
Decimation FAPC	**-55**	**-36**
Contiguous FAPC	**-56**	**-42**

4.2.4 Dense Scenario with Doppler

Finally, the result for a dense environment with randomly distributed Doppler shifts is considered. The largest Doppler shift is equivalent to that induced by a Mach 6 scatterer illuminated by a 1 μs pulse at S band. Figures 4.20

and 4.21 illustrate the results when $M = 4$ ($K = 15$) for decimation and contiguous FAPC, respectively, when 3 adaptive stages are performed. The decimation FAPC and APC algorithms suffer from Doppler mismatch and thus exhibit some Doppler induced range sidelobes. However, contiguous FAPC exhibits almost no Doppler-induced range sidelobes and accurately estimates all scatterers. Note that contiguous FAPC may exhibit some small spurious peaks, which have been observed to follow the envelope of APC's Doppler induced sidelobes, as seen in Figure 4.21 range index 63. The MSE results for this case can be seen in Table IV.

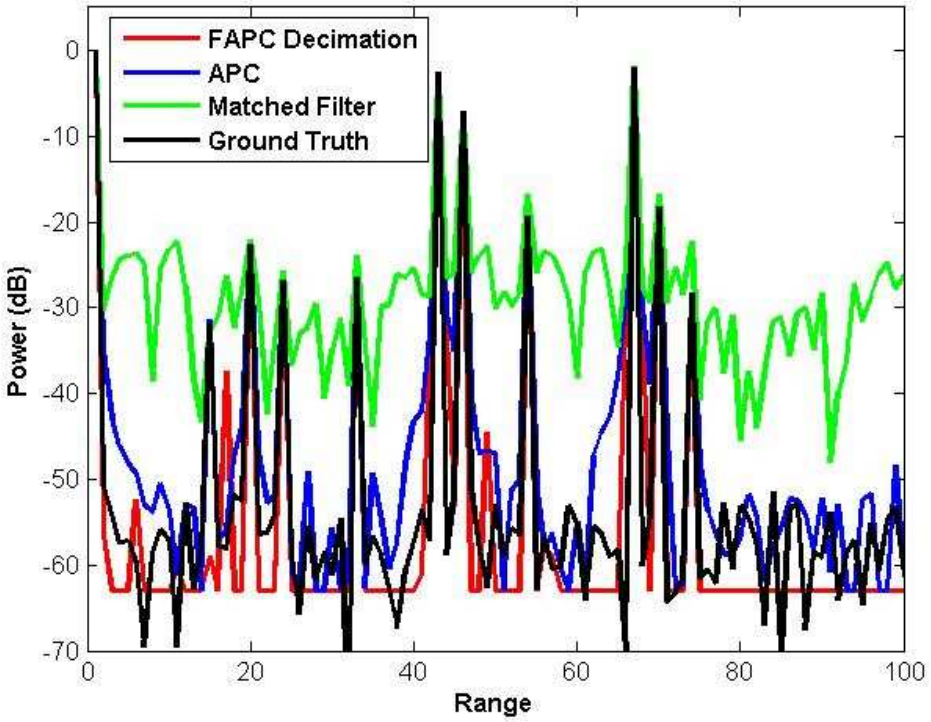

Figure 4.20 Dense Scenario with Doppler, Decimation FAPC, *M = 4*

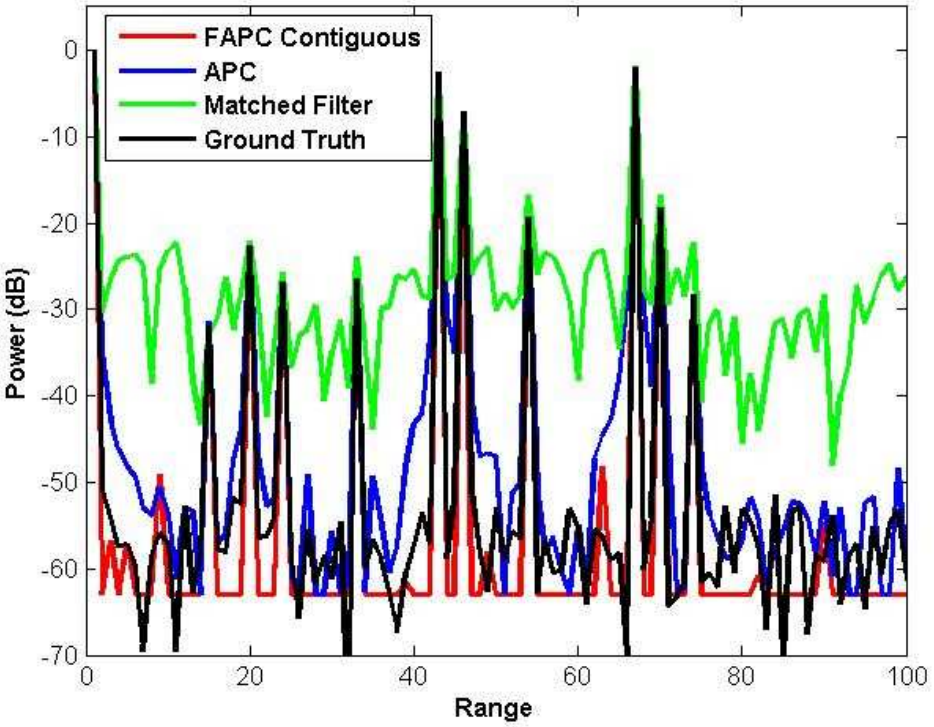

Figure 4.21 Dense Scenario with Doppler, Contiguous FAPC, *M = 4*

Table IV MSE Results in dB**,** Dense Scenario with Doppler

	M = 4
Matched Filter	**-28**
APC	**-36**
Decimation FAPC	**-36**
Contiguous FAPC	**-37**

4.2.5 Probability of Detection

The results shown above for Fast APC are anecdotal and do not fully characterize the performance of the algorithm. To provide a more concrete analysis of the new algorithm probability of detection results were obtained for APC, the normalized matched filter, and both versions of Fast APC by averaging

results over 1,000 trials for a range profile containing a sidelobe-masked target. The range profile contains a single large target with an SNR of 60 dB and a smaller masked target that, for each trial, is randomly assigned to a nearby range cell masked by the sidelobes of the large target. The SNR of the small target was varied to obtain the probability of detection curves shown in Figs. 4.22 and 4.23 for decimation and contiguous FAPC, respectively. A Cell-Averaging Constant False Alarm Rate (CA-CFAR) detector [19] was used with a probability of false alarm of 10^{-6}. The range cells included in the determination of the CA-CFAR threshold are the $2N-2$ range cells that coincide with the sidelobes of the large target excluding the range cell in which the small masked target resides.

The matched filter performs poorly when the signal power of the small target is not sufficiently higher than the sidelobes induced by the large target. The sidelobe suppression capability of the APC algorithm uncovers the masked scatterer and yields more than a 30 dB improvement over the matched filter for a probability of detection of 50%. Both versions of the Fast APC algorithm are found to degrade gracefully as M increases with M = 10, for example, still yielding a 15 dB improvement for decimation FAPC and a 17 dB improvement for contiguous FAPC relative to the matched filter for a probability of detection of 50%. The probability of detection results combined with the computational cost plot in Fig. 3.5 offer an accurate illustration of the performance/computation trade-off achieved with Fast APC.

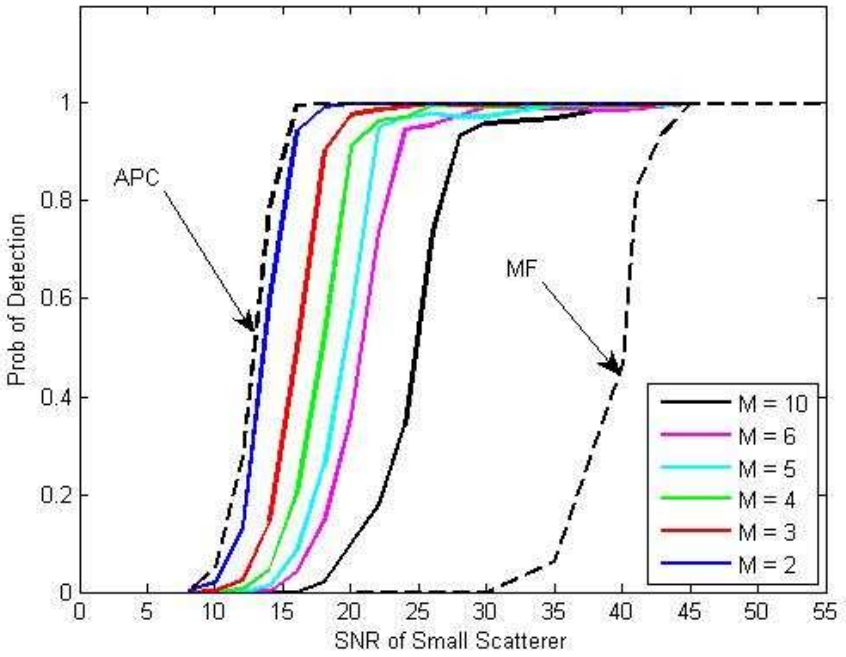

Figure 4.22 Probability of Detection Results, Decimation FAPC

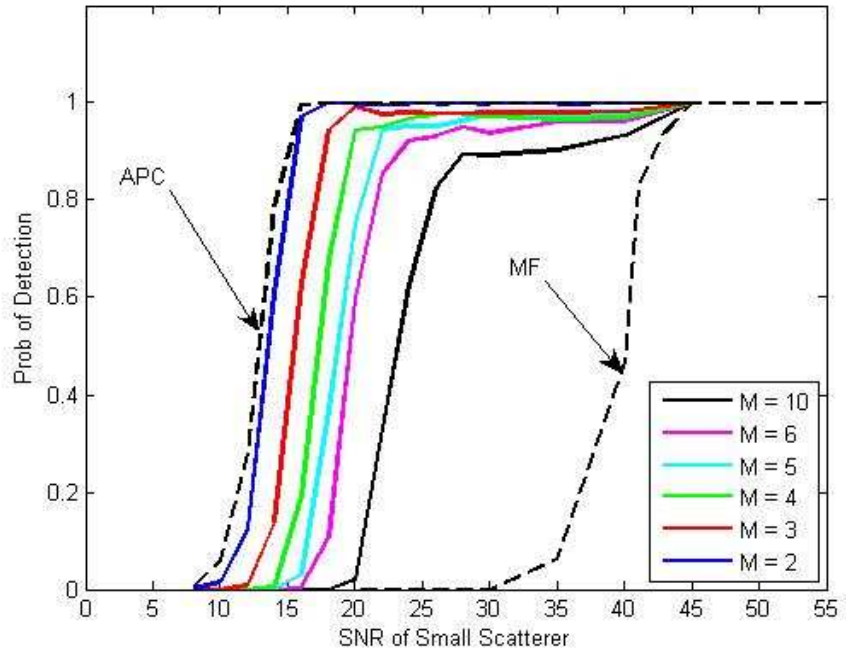

Figure 4.23 Probability of Detection Results, Contiguous FAPC

CHAPTER 5 CONCLUSIONS AND FUTURE WORK

5.1 Conclusions

The motivation for the work done in this thesis was to explore the increased and reduced dimensionality aspects of the Adaptive Pulse Compression (APC) algorithm. Over-sampling the transmitted waveform and received signal results in an increased-dimensionality form of APC capable of achieving range super-resolution on a single pulse basis. Conversely, segmenting the APC cost function resulted in a new algorithm, namely Fast APC, capable of range sidelobe suppression at a significantly lower computational cost.

The over-sampled APC algorithm and Least-Squares approach are capable of achieving range super-resolution which offers many benefits to pulsed radar systems. Continuous and realistic discrete waveforms were examined and it was determined that the extraneous bandwidth possessed by the transition regions of the discrete phase waveform provided superior performance to the continuous waveform. Straddling loss was shown to be improved by over-sampling and diagonal loading was successfully utilized to alleviate ill-conditioning effects created by over-sampling the transmit waveform used for processing.

Much work has been done in the field of pulse compression to design waveforms and filters which possess desirable sidelobe characteristics. The previously developed APC algorithm [12] is capable of almost complete range

sidelobe suppression by employing a unique pulse compression filter at each range cell of interest. However, APC incurs a high computational cost in terms of current processing power. Fast Adaptive Pulse Compression was derived by applying decimation and contiguous blocking techniques to the full-dimension MMSE structure. The new algorithm is computationally efficient and provides sensitivity on the level of APC when the segmenting factor is not extreme. In addition, the contiguous embodiment of Fast APC exhibits improved Doppler tolerance compared to the decimation FAPC and APC algorithms.

5.2 Future Work

The work done in this thesis has generated several new research opportunities:

- Application of over-sampled APC and Fast APC to real data which perhaps may lead to exploring implementation of the Fast APC algorithm in a real-time system
- Combining Fast APC and over-sampled APC, *i.e.* achieving range super-resolution at a reduced computational cost
- Examining other embodiments of Fast APC, *i.e.* different segmenting methods or combinations of segmentation schemes
- Enhancing robustness of Fast APC to limit over-suppression and mismatch loss

References

[1] S. Kingsley and S. Quegan, *Understanding Radar Systems*, SciTech Publishing, Inc., 1999, pp. 145-155.

[2] M.I. Skolnik, *Introduction to Radar Systems*, McGraw-Hill, 1980, pp. 276-278, 349-376, and pp. 420-434.

[3] B.L. Lewis and F.F. Kretschmer, Linear frequency modulation derived polyphase pulse compression codes," *IEEE Trans. Aerospace and Electronic Systems*, Vol. AES-18, No. 5, pp. 637-641, Sept. 1982.

[4] Nathanson, F.E. *Radar Design Principles.* 2nd ed. New York: McGraw-Hill, 1991, Sec. 13.11.

[5] Farnett, E.C., and G.H. Stevens. "Pulse Compression Radar" In *Radar Handbook*, 2nd ed. M. Skolnik (Ed.) New York: McGraw-Hill, 1990, Sec. 10.4.

[6] Costas, J.P. "A Study of a Class of Detection Waveforms Having Nearly Ideal Range-Doppler Ambiguity Properties." *Proc. IEEE* 72 (August 1984), pp 996-1009.

[7] N. Levanon, *Radar Principles*, John Wiley & Sons, Inc., 1988, pp. 159-162

[8] Frank, F.L. "Polyphase Codes with Good Nonperiodic Correlation Properties." *IEEE Trans.* IT-9 (January 1963), pp. 43-45.

[9] T. Felhauer, "Digital signal processing for optimum wideband channel estimation in the presence of noise," *IEE Proceedings-F,* vol. 140, no. 3, pp. 179-186, June 1993.

[10] Daniels, R.C., Gregers-Hansen, Vilhelm "Code Inverse Filtering for Complete Sidelobe Removal in Binary Phase Coded Pulse Compression Systems," *Intl. Radar Confrence*, pp. 256-261, May 2005.

[11] M.H. Ackroyd and F. Ghani, "Optimum mismatched filter for sidelobe suppression," *IEEE Trans. Aerospace and Electronic Systems*, Vol. AES-9, pp. 214-218, March 1973.

[12] S.D. Blunt and K. Gerlach, "Adaptive pulse compression via MMSE estimation," *IEEE Trans. Aerospace and Electronic Systems*, Vol. AES-42, No. 2, pp. 572-584, April. 2006.

[13] J. G. Proakis and D.G. Manolakis, *Digital Signal Processing Principles, Algorithms, and Applications*, Prentice-Hall, 1996, pp. 952-955.

[14] W.F. Gabriel, "Superresolution techniques in the range domain," Proc. *IEEE Intl. Radar Conf.*, May 1990, pp. 263-267.

[15] W.F. Gabriel, "Improved range superresolution via bandwidth extrapolation," Proc. *IEEE National Radar Conf.*, Apr. 1993, pp. 123-127.

[16] S. Liu and J. Xiang, "Novel method for superresolution in radar range domain," *IEE Proc. Radar, Sonar, Navig.,* vol. 146, no. 1, Feb. 1999, pp. 40-44.

[17] J. Ward, "Space-time adaptive processing for airborne radar", *Lincoln Laboratory Technical Report*, ESC-TR-94-109.

[18] T.K. Moon and W.C. Stirling, *Mathematical Methods and Algorithms for Signal Processing*, Prentice Hall, 2000, pg. 258.

[19] P.P. Gandhi and S.A. Kassam, "Analysis of CFAR Processors in Nonhomogeneous Background," *IEEE Trans. Aerospace and Electronic Systems*, Vol. AES-24, No. 4, pp. 427-445, July 1988.